NATIONAL ADVISORY COMMITTEE FOR AERONAUTICS

TECHNICAL NOTE 2367

GENERAL PLASTIC BEHAVIOR AND APPROXIMATE SOLUTIONS OF ROTATING DISK IN STRAIN-HARDENING RANGE

By M. H. Lee Wu

Lewis Flight Propulsion Laboratory
Cleveland, Ohio

NACA

Washington

May 1951

NATIONAL ADVISORY COMMITTEE FOR AERONAUTICS

TECHNICAL NOTE 2367

GENERAL PLASTIC BEHAVIOR AND APPROXIMATE SOLUTIONS OF ROTATING DISK IN STRAIN-HARDENING RANGE

By M. H. Lee Wu

SUMMARY

A partly linearized solution of plastic deformation of a rotating disk based on the deformation theory of plasticity and considering finite strains is obtained. The stresses and the strains of this problem for a given material and a given maximum strain can be obtained merely by a simple multiplication using the tables presented herein. This method is used to investigate the general plastic behavior of a rotating disk. An approximate method is also given in which the stresses are calculated by using strains obtained from the ideally plastic material and the tensile true stress-strain curve of the material.

Numerical examples are calculated by the two methods and agree very well with the exact solution based on deformation theory previously obtained. Calculations are also made for ideally plastic material and for the power-function approximation for purposes of comparison.

The following conclusions, similar to those resulting from the linearized solution of the thin plate with a circular hole, are obtained for this problem:

(1) The variation of a parameter, which is determined from the octahedral shear stress-strain curve of the material, can be used as a general criterion of the applicability of deformation theory.

(2) The ratios of strain along the radius to the maximum value and the ratios of principal stresses are essentially independent of the octahedral shear stress-strain curve of the material, but the distributions of the stresses, and therefore the rotating speeds of the disk, depend very much on the material.

(3) The results obtained from the ideally plastic material with the infinitesimal strain concept give good approximate values of strains but not of stresses.

(4) The rotating speed of the disk for a given maximum strain of the disk can be determined directly from the tensile true stress-strain curve of the material.

(5) Good correlation between the experimentally determined bursting speed and the calculated value determined directly from the tensile stress-strain curve of the material is obtained.

(6) If a simple analytical function representing the octahedral shear stress-strain relation is required for analysis, the power-law approximation can be used.

INTRODUCTION

In the design of a high-speed or a highly stressed machine member such as a turbine or a compressor rotor, the distributions of stresses and strains in the strain-hardening range must be known. The problem of a rotating disk for an ideally plastic material was solved by Nadai (reference 1). A solution for gas-turbine disks considering small plastic strain in the strain-hardening range is obtained in reference 2 by a trial-and-error procedure and by using elastic stress and strain distributions as a first approximation. An experimental investigation for the high-speed rotating disk is made in reference 3; distributions of plastic strains (logarithmic strains) for different types of disk are measured. The effect of strength and ductility on the burst characteristics of rotating disks are experimentally investigated in reference 4. An exact solution based on deformation theory for plane plastic stress problems with axial symmetry (including a circular membrane under pressure, a rotating disk, and a thin plate with a circular hole) in the strain-hardening range is obtained in reference 5; numerical calculations are made for Inconel X and Timken alloy 16-25-6. A linearized solution of plastic deformation of a thin plate with a circular hole is given in reference 6. This linearized solution is not only simple and accurate but also offers a means of investigating the general plastic behavior of that problem for most materials.

Extension of this method to the problem having the additional complication of body forces, such as a rotating disk, is therefore interesting. (For a circular membrane under pressure, the normal pressure can be treated in a manner similar to the centrifugal force of a rotating disk.) The partly linearized solution obtained at the NACA Lewis laboratory and presented herein is also used to investigate general plastic behavior for this problem.

SYMBOLS

The following symbols are used in this report:

A,B,C, D,E,F	coefficients of nonlinear differential equations; functions of α, γ, and r/k
b	original outer radius of rotating disk
H,J,L	trigonometric functions of α
h	instantaneous thickness of disk
h_{init}	initial thickness of disk
K	strain-hardening constant
K_1	arbitrary loading constant
k	constant, in dimension of length
m	parameter relating to strain hardening
n	parameter relating to criterion of applicability of deformation theory
r	radial coordinate of undeformed disk
u	radial displacement
z	axial coordinate
α	parameter indicating ratio of principal stresses
γ	octahedral shear strain
ϵ	logarithmic strain (natural strain), logarithm of instantaneous length divided by initial length of element
θ	angular coordinate
ρ	mass per unit volume
σ	normal true stress, force per unit instantaneous area
τ	octahedral shear stress
ω	angular velocity

Subscripts:

b	at outer radius b
o	at center of disk
r,θ,z	principal directions: radial, tangential, and axial directions

BASIC EQUATIONS

A disk having an original outer radius b and an initial thickness h_{init} rotating about its axis with an angular velocity ω is shown in figure 1(a). A small element defined by $\Delta\theta$ and $\Delta(r+u)$ taken at the radius $(r+u)$ in the deformed state is given in figure 1(b). In the undeformed state, this element is located at r and defined by $\Delta\theta$ and Δr. The instantaneous thickness h of the element and the stresses acting on the element are also shown in the figure.

The relations of stresses and strains based on the deformation theory for plane plastic stress in the cylindrical coordinates are (references 7 and 8):

$$\epsilon_r + \epsilon_\theta + \epsilon_z = 0 \tag{1}$$

$$\tau = \tau(\gamma) \tag{2}$$

$$\tau = \frac{\sqrt{2}}{3}\left(\sigma_r^2 - \sigma_r \sigma_\theta + \sigma_\theta^2\right)^{\frac{1}{2}} \tag{3a}$$

$$\gamma = 2\sqrt{\frac{2}{3}}\left(\epsilon_r^2 + \epsilon_r \epsilon_\theta + \epsilon_\theta^2\right)^{\frac{1}{2}} \tag{3b}$$

$$\epsilon_r = \frac{1}{3}\frac{\gamma}{\tau}\left(\sigma_r - \frac{1}{2}\sigma_\theta\right) \tag{4a}$$

$$\epsilon_\theta = \frac{1}{3}\frac{\gamma}{\tau}\left(\sigma_\theta - \frac{1}{2}\sigma_r\right) \tag{4b}$$

$$\epsilon_z = \frac{1}{3}\frac{\gamma}{\tau}\left[-\frac{1}{2}\left(\sigma_r + \sigma_\theta\right)\right] \tag{4c}$$

The constants 1/2 and 1/3 in equations (4) are determined from the condition defined by equation (1) and one of the equations (3). Only five of these equations are therefore independent.

The finite-strain concept (references 8 to 10), which considers the instantaneous dimensions of the element, is used because large deformation in the strain-hardening range is considered. The stress is then equal to the force divided by the instantaneous area and the strain to the logarithm of the instantaneous length divided by the initial length of the element (references 8 to 10). It is mentioned in reference 5 that as long as the deformation theory is applicable, the logarithmic strain can also be used. The strain-displacement relations for this problem are then as follows:

$$\epsilon_r = \log_e \frac{d(r+u)}{dr} \tag{5a}$$

$$\epsilon_\theta = \log_e \frac{r+u}{r} \tag{5b}$$

$$\epsilon_z = \log_e \frac{h}{h_{init}} \tag{5c}$$

From the condition of equilibrium in the radial direction of the small element in figure 1(b), the following equation of equilibrium is obtained (reference 5):

$$(r+u) \frac{d(\sigma_r h)}{d(r+u)} = (\sigma_\theta - \sigma_r)\, h - \rho\, (\omega r)^2\, h_{init} \frac{r+u}{r} \frac{dr}{d(r+u)} \tag{6}$$

Nine equations defining this problem are equations (1), (2), (3b), (4a), (4b), (5a), (5b), (5c), and (6), which involve nine unknowns: σ_r, σ_θ, ϵ_r, ϵ_θ, ϵ_z, γ, τ, h, and u. Equations (1) and (5) can be used to eliminate ϵ_z, u, and h, resulting in a compatibility equation. The equations defining this problem are then reduced to six equations with six unknowns: σ_r, σ_θ, ϵ_r, ϵ_θ, γ, and τ. Two of the four unknowns, σ_r, σ_θ, ϵ_r, and ϵ_θ, may be eliminated by using equations (4a) and (4b) or (3b). The quantity τ is a known function of γ, which is experimentally determined from a simple tensile test. The problem is then reduced to one involving three unknowns. Obtaining the solution of the resulting equations is not, however, a simple matter. This difficulty can be avoided by using the following transformation (references 1 and 5 to 7) because the yielding surface of plane plastic stress based on the deformation theory is an ellipse:

$$\sigma_\theta + \sigma_r = 3\sqrt{2}\,\tau \sin\alpha$$

$$\sigma_\theta - \sigma_r = \sqrt{6}\,\tau \cos\alpha$$

Rewriting the principal stresses as functions of τ and α gives

$$\left.\begin{aligned}\sigma_r &= \sqrt{\frac{3}{2}}\,\tau\,(\sqrt{3}\sin\alpha - \cos\alpha)\\ \sigma_\theta &= \sqrt{\frac{3}{2}}\,\tau\,(\sqrt{3}\sin\alpha + \cos\alpha)\end{aligned}\right\} \qquad (7)$$

where τ, which is a function of γ, varies with r and also with load. With equations (7) substituted into equations (4a) and (4b), the principal strains can be expressed as functions of γ and α as follows:

$$\left.\begin{aligned}\epsilon_r &= \frac{\gamma}{2\sqrt{2}}\,(\sin\alpha - \sqrt{3}\cos\alpha)\\ \epsilon_\theta &= \frac{\gamma}{2\sqrt{2}}\,(\sin\alpha + \sqrt{3}\cos\alpha)\end{aligned}\right\} \qquad (8)$$

In these equations, the parameter α is closely related to the ratio of principal stresses, inasmuch as

$$\frac{\sigma_r}{\sigma_\theta} = \frac{\sqrt{3}\sin\alpha - \cos\alpha}{\sqrt{3}\sin\alpha + \cos\alpha}$$

and varies almost linearly with α for the range of α encountered in the present problem, which is the same range as in the thin plate with a circular hole as shown in figure 2 of reference 6. By using the transformation, the equations for this problem are reduced to the following two nonlinear differential equations, which are to be solved with an experimentally determined function $\tau(\gamma)$:

$$A\left(\frac{r}{k}\right)\frac{d\alpha}{d\left(\frac{r}{k}\right)} + B\left(\frac{r}{k}\right)\frac{d\gamma}{d\left(\frac{r}{k}\right)} = C$$

$$D\left(\frac{r}{k}\right)\frac{d\alpha}{d\left(\frac{r}{k}\right)} + E\left(\frac{r}{k}\right)\frac{d\gamma}{d\left(\frac{r}{k}\right)} = F$$

or

$$\left.\begin{aligned}\left(\frac{r}{k}\right)\frac{d\alpha}{d\left(\frac{r}{k}\right)} &= \frac{CE - FB}{AE - DB}\\ \left(\frac{r}{k}\right)\frac{d\gamma}{d\left(\frac{r}{k}\right)} &= \frac{FA - CD}{EA - BD}\end{aligned}\right\} \tag{9}$$

where

$$\left.\begin{aligned}A &= (\sqrt{3}\cos\alpha + \sin\alpha) - (\sqrt{3}\sin\alpha - \cos\alpha)\frac{\gamma\cos\alpha}{\sqrt{2}}\\ B &= (\sqrt{3}\sin\alpha - \cos\alpha)\left(\frac{\gamma}{\tau}\frac{d\tau}{d\gamma} - \frac{\gamma\sin\alpha}{\sqrt{2}}\right)\frac{1}{\gamma}\\ C &= 2(\cos\alpha)\,e^{\left(-\sqrt{\frac{3}{2}}\gamma\cos\alpha\right)} - \sqrt{\frac{2}{3}}\rho(\omega k)^2\frac{1}{\tau}\left(\frac{r}{k}\right)^2 e^{\frac{\gamma}{\sqrt{2}}\sin\alpha}\\ D &= (\sqrt{3}\sin\alpha - \cos\alpha)\gamma\\ E &= -(\sqrt{3}\cos\alpha + \sin\alpha)\\ F &= 2\sqrt{2}\left[1 - e^{\left(-\sqrt{\frac{3}{2}}\gamma\cos\alpha\right)}\right]\end{aligned}\right\} \tag{9a}$$

Using equations (9a) and expanding the terms of $e^{f(\gamma,\alpha)}$ into a series result in

$$\left.\begin{aligned}CE - BF &= -2HL - 2\sqrt{3}\,HJ\left(\frac{\gamma}{\tau}\frac{d\tau}{d\gamma} - \sqrt{\frac{3}{2}}\frac{1}{J}\frac{\gamma}{\gamma_o}\gamma_o\right)f_1(\alpha,\gamma) + LK_1\left(\frac{\tau_o}{\tau}\right)\left(\frac{r}{k}\right)^2 f_2(\alpha,\gamma)\\ AF - CD &= \left\{8H^2 - 2\sqrt{3}\,HL\left[1 - f_1(\alpha,\gamma)\right] + JK_1\left(\frac{\tau_o}{\tau}\right)\left(\frac{r}{k}\right)^2 f_2(\alpha,\gamma)\right\}\gamma\\ AE - BD &= -L^2 - J^2\left(\frac{\gamma}{\tau}\frac{d\tau}{d\gamma} - \sqrt{\frac{3}{2}}\frac{1}{J}\frac{\gamma}{\gamma_o}\gamma_o\right)\end{aligned}\right\} \tag{9b}$$

where

$$f_1(\alpha,\gamma) = \frac{1}{\sqrt{\frac{3}{2}}(\cos\alpha)\gamma}\left[1 - e^{-\sqrt{\frac{3}{2}}(\cos\alpha)\gamma}\right]$$

$$= 1 - \frac{1}{2}\sqrt{\frac{3}{2}}(\cos\alpha)\,\gamma + \frac{1}{4}(\cos^2\alpha)\,\gamma^2 \ldots$$

$$f_2(\alpha,\gamma) = e^{\frac{\gamma}{\sqrt{2}}\sin\alpha}$$

$$= 1 + \left(\frac{1}{\sqrt{2}}\sin\alpha\right)\gamma + \frac{1}{2}\left(\frac{1}{\sqrt{2}}\sin\alpha\right)^2\gamma^2 + \frac{1}{6}\left(\frac{1}{\sqrt{2}}\sin\alpha\right)^3\gamma^3 + \ldots$$

$$H = \cos\alpha$$

$$J = \sqrt{3}\sin\alpha - \cos\alpha$$

$$K_1 = \sqrt{\frac{2}{3}}\frac{\rho(\omega k)^2}{\tau_o}$$

$$L = \sqrt{3}\cos\alpha + \sin\alpha$$

LINEARIZATION OF EQUATIONS

In equations (9b), the variable τ occurs not only in the combination of $\frac{\gamma}{\tau}\frac{d\tau}{d\gamma}$ as in the case of a thin plate with a circular hole (reference 6), but also in the loading term. As proposed in reference 6, the term $\frac{\gamma}{\tau}\frac{d\tau}{d\gamma}$ can be replaced by m, which is equal to the slope of a straight line approximating the $\tau(\gamma)$ curve on the logarithmic plot within the range of γ encountered along the radius of the disk, γ_b to γ_o. Thus m is a function of γ_o; in other words, the value of m for one material is different for different loads. The special case where a straight line is used to approximate the whole strain-hardening range of the $\tau(\gamma)$ curve of a given material on the logarithmic plot, so that m is constant through the strain-hardening range, is the well-known power-law approximation. As in the case of a thin plate with a circular

hole, the power-law approximation gives very good approximate results for this problem, as will be shown in the section "Calculations, Results, and Discussion." The term $\frac{\gamma}{\tau}\frac{d\tau}{d\gamma}$ can thus be replaced by m without appreciable error.

Furthermore, the term $\sqrt{\frac{3}{2}}\frac{1}{J}\left(\frac{\gamma}{\gamma_o}\right)$ in equations (9b) can be replaced by a constant C_1, which is determined in a manner similar to that in the case of a thin plate with a circular hole (reference 6), as will be described. The terms $\left(\frac{\gamma}{\tau}\frac{d\tau}{d\gamma} - \sqrt{\frac{3}{2}}\frac{1}{J}\frac{\gamma}{\gamma_o}\gamma_o\right)$ in equations (9b) then become $(m - C_1\gamma_o)$.

The general information concerning the effect of the $\tau(\gamma)$ curve of the material on the solution of this problem can be obtained only if the quantity τ/τ_o in the loading term can possibly be expressed as a function of $(m - C_1\gamma_o)$. For any part of the $\tau(\gamma)$ curve that does not deviate greatly from a straight line in the strain-hardening range within the value of γ considered, γ_o to γ_b, the following equation can be written with sufficient accuracy:

$$\tau = \tau_o - (\gamma_o - \gamma)\left(\frac{d\tau}{d\gamma}\right)_{av} = \tau_o\left[1 - \left(1 - \frac{\gamma}{\gamma_o}\right)\frac{\gamma_o}{\tau_o}\left(\frac{d\tau}{d\gamma}\right)_{av}\right] \quad (10)$$

where $\left(\frac{d\tau}{d\gamma}\right)_{av}$ is the average slope of $\tau(\gamma)$ from γ_o to γ_b and (γ_o, τ_o) is a known point on the $\tau(\gamma)$ curve. The quantity $\frac{\gamma_o}{\tau_o}\left(\frac{d\tau}{d\gamma}\right)_{av}$ does not equal $(m - C_1\gamma_o)$ but has a certain relation to it. Results obtained in reference 5 show that the values of α and γ/γ_o are not very sensitive to the $\tau(\gamma)$ curve of the material. If only a linear relation between $\frac{\gamma_o}{\tau_o}\left(\frac{d\tau}{d\gamma}\right)_{av}$ and $(m - C_1\gamma_o)$ is retained, equation (10) becomes

$$\frac{\tau}{\tau_o} = 1 - \left(1 - \frac{\gamma}{\gamma_o}\right)C_2\,(m - C_1\gamma_o) \quad (10a)$$

An approximate value of $C_1 = 0.5$, which is equal to the mean value of $\sqrt{\frac{3}{2}}\frac{1}{J}\frac{\gamma}{\gamma_o}$ along the radius, can be used in equation (10a). The values of γ_o, γ_b/γ_o, and m are known for any point (γ_o, τ_o). By using the values of $\tau/\tau_o = \tau_b/\tau_o$ taken from the true octahedral shear stress-strain curves of several materials and using equation (10a) and $\gamma/\gamma_o = \gamma_b/\gamma_o$, the constant C_2 is then found to be

$$C_2 = 2$$

A zero value of C_2 is used for the case of negative $(m - C_1\gamma_o)$, because there is no negative slope on the true stress-strain curve of any material. Thus:

$$\frac{\tau}{\tau_o} = 1 - 2\left(1 - \frac{\gamma}{\gamma_o}\right)(m - C_1\gamma_o) \qquad (10b)$$

It may be noted that this relation is very approximate and is only used to determine the variations of α and γ/γ_o along the radius, which are not sensitive to the $\tau(\gamma)$ curve of the material. For the stress and rotating speed, which are dependent on the $\tau(\gamma)$ curve, this approximate relation cannot be used. The stresses are determined from the values of α and γ/γ_o obtained by the partly linearized solution and the true octahedral shear stress-strain curve of the material obtained from the tensile test. The rotating speed is determined from the distributions of tangential stress and strain.

Substituting equation (10b) into equations (9b) and the resulting equation into equations (9), replacing $\left(\frac{\gamma}{\tau}\frac{d\tau}{d\gamma} - \sqrt{\frac{3}{2}}\frac{1}{J}\frac{\gamma}{\gamma_o}\gamma_o\right)$ by $(m - C_1\gamma_o)$, and neglecting the small terms (as in reference 6), the following equations are obtained:

$$\left.\begin{aligned}
\frac{d\alpha}{d\left(\frac{r}{k}\right)} &= \frac{2H}{L}\,\frac{1+\frac{\sqrt{3}J}{L}(m-C_1\gamma_o)-\frac{K_1}{2H}\left(\frac{r}{k}\right)^2\left[1-2\left(1-\frac{\gamma}{\gamma_o}\right)(m-C_1\gamma_o)\right]^{-1}}{\left[1+\left(\frac{J}{L}\right)^2(m-C_1\gamma_o)\right]\left(\frac{r}{k}\right)} \\
\frac{d\left(\frac{\gamma}{\gamma_o}\right)}{d\left(\frac{r}{k}\right)} &= -\frac{8H^2}{L^2}\,\frac{\left\{1-\frac{JK_1}{8H^2}\left(\frac{r}{k}\right)^2\left[1-2\left(1-\frac{\gamma}{\gamma_o}\right)(m-C_1\gamma_o)\right]^{-1}\right\}\frac{\gamma}{\gamma_o}}{\left[1+\left(\frac{J}{L}\right)^2(m-C_1\gamma_o)\right]\left(\frac{r}{k}\right)}
\end{aligned}\right\} \quad (11)$$

Let

$$n = m - C_1\gamma_o \quad (12)$$

In equation (12), once the value of γ_o is chosen, m can be determined from the $\tau(\gamma)$ curve of the material; C_1 is a constant and n is therefore a constant determined from the $\tau(\gamma)$ curve of the material. Substituting equation (12) into equations (11) gives

$$\left.\begin{aligned}
\frac{d\alpha}{d\left(\frac{r}{k}\right)} &= \frac{2H}{L}\,\frac{1+\sqrt{3}\,\frac{J}{L}n-\frac{K_1}{2H}\left[1-2\left(1-\frac{\gamma}{\gamma_o}\right)n\right]^{-1}\left(\frac{r}{k}\right)^2}{\left[1+\left(\frac{J}{L}\right)^2 n\right]\left(\frac{r}{k}\right)} \\
\frac{d\left(\frac{\gamma}{\gamma_o}\right)}{d\left(\frac{r}{k}\right)} &= -\frac{8H^2}{L^2}\,\frac{\left\{1-\frac{JK_1}{8H^2}\left[1-2\left(1-\frac{\gamma}{\gamma_o}\right)n\right]^{-1}\left(\frac{r}{k}\right)^2\right\}\left(\frac{\gamma}{\gamma_o}\right)}{\left[1+\left(\frac{J}{L}\right)^2 n\right]\left(\frac{r}{k}\right)}
\end{aligned}\right\} \quad (13)$$

In equations (13), all the terms are functions of α, γ/γ_o, and r/k except K_1, which is an arbitrary loading constant, and n, which is also a constant during the calculation. The values of α

and γ/γ_o can be obtained along r/k until α reaches the value that satisfies the outer boundary condition $\left(\alpha = \frac{\pi}{6}\right)$. Because r at the outer boundary is equal to b, the constant k can be determined. (For details, see reference 5.) The variations of α and γ/γ_o with r/b for different values of n can then be calculated. Compare the values of α and γ/γ_o along r/b obtained from equations (13) for several values of n with the values of α and γ/γ_o along r/b obtained in reference 5. (The values of n for these last cases are calculated from equation (12) with the approximate value $C_1 = 0.5$.) The variations of α and γ/γ_o with r/b having the same n values obtained from equations (13) and from reference 5 are quite close; therefore $C_1 = 0.5$ can be used and equation (12) becomes

$$n = m - 0.5\,\gamma_o \tag{12a}$$

The relations of α and γ/γ_o with r/b for several values of n are given in both tabular and curve form to facilitate solution of this problem for any material under any maximum strain. This method of determining the distributions of α and γ/γ_o along r/b will be referred to as the "partly linearized solution."

PRINCIPAL STRESSES AND STRAINS

After the variations of α and γ/γ_o with r/b are obtained by the partly linearized solution, the principal stresses and strains can be obtained from equations (7) and (8) together with the actual τ and γ relation of a given material. The equations show that ϵ_r/γ, ϵ_θ/γ, σ_r/τ, and σ_θ/τ are functions of α only; they can be calculated for different values of α and given in tabular form to facilitate solution of any given case. Equations (7) and (8) can be written as

$$\left.\begin{aligned} \sigma_r/\tau &= \sqrt{\frac{3}{2}}\left(\sqrt{3}\sin\alpha - \cos\alpha\right) \\ \sigma_\theta/\tau &= \sqrt{\frac{3}{2}}\left(\sqrt{3}\sin\alpha + \cos\alpha\right) \end{aligned}\right\} \tag{7a}$$

$$\left.\begin{aligned} \epsilon_r/\gamma &= \frac{1}{2\sqrt{2}}(\sin\alpha - \sqrt{3}\cos\alpha) \\ \epsilon_\theta/\gamma &= \frac{1}{2\sqrt{2}}(\sin\alpha + \sqrt{3}\cos\alpha) \end{aligned}\right\} \qquad (8a)$$

The values of principal stresses and strains can then be obtained by simple multiplication.

It is usually interesting to know the ratios of maximum and minimum tangential stress and strain, because the rotating speed of the disk is mainly determined by the tangential stress and strain along the radius. The maximum tangential stress and strain occur at the center of the disk; at $r = 0$,

$$\sigma_\theta = \sigma_r$$

$$\alpha_o = \frac{\pi}{2}$$

The minimum tangential stress and strain occur at the rim of the disk; at $r = b$,

$$\sigma_r = 0$$

$$\alpha_b = \frac{\pi}{6}$$

From equations (7), the ratio of maximum to minimum tangential stress is

$$\frac{(\sigma_\theta)_o}{(\sigma_\theta)_b} = \frac{\tau_o(\sqrt{3}\sin\frac{\pi}{2} + \cos\frac{\pi}{2})}{\tau_b(\sqrt{3}\sin\frac{\pi}{6} + \cos\frac{\pi}{6})} = \frac{\tau_o}{\tau_b}$$

From equations (8), the ratio of maximum to minimum tangential strain is

$$\frac{(\epsilon_\theta)_o}{(\epsilon_\theta)_b} = \frac{\gamma_o(\sin\frac{\pi}{2} + \sqrt{3}\cos\frac{\pi}{2})}{\gamma_b(\sin\frac{\pi}{6} + \sqrt{3}\cos\frac{\pi}{6})} = \frac{\gamma_o}{2\gamma_b}$$

IDEALLY PLASTIC AND APPROXIMATE SOLUTION

For the case of $n = 0$, equations (13) become

$$\frac{d\alpha}{d\left(\frac{r}{k}\right)} = \left(\frac{2H}{L}\right) \frac{1 - \frac{K_1}{2H}\left(\frac{r}{k}\right)^2}{\left(\frac{r}{k}\right)} \tag{13a}$$

$$\frac{d\,\frac{\gamma}{\gamma_o}}{d\left(\frac{r}{k}\right)} = \left(-\frac{8H^2}{L^2}\right) \frac{\left[1 - \frac{JK_1}{8H^2}\left(\frac{r}{k}\right)^2\right]\left(\frac{\gamma}{\gamma_o}\right)}{\left(\frac{r}{k}\right)} \tag{13b}$$

Equations (13a) and (13b) can be integrated numerically; these equations are much simpler than those for the cases of $n \neq 0$. For ideally plastic material with the infinitesimal strain concept, γ_o is infinitesimal and $m = 0$; the constant n is then equal to zero; this case is a special one of $n = 0$. For this case, Nadai (reference 1) obtained a similar relation between α and r/b as equation (13a).

Equations (13a) and (13b) can also be used to determine approximately the variations of α and γ/γ_o with r/b for a material with $n \neq 0$. An approximate method of solution is therefore proposed. The procedure of the approximate solution is as follows: Use the variations of α and γ/γ_o with r/b for $n = 0$ (or for ideally plastic material with infinitesimal strain) as the approximate solution of the variations of α and γ/γ_o with r/b. The principal strains ϵ_θ and ϵ_r can be calculated from the approximate relations of α, γ/γ_o, and r/b because the strains are functions of α and γ only. The stresses, which are functions of α and τ, can be calculated from equations (7a) by using the tensile true $\tau(\gamma)$ curve of the material and the relations of α, γ/γ_o, and r/b determined for $n = 0$.

DETERMINATION OF ROTATING SPEED OF DISK

The rotating-speed function $\rho(\omega b)^2$ can be determined by considering a circular sector as shown in figure 1(c). The radial component of force acting on the sector due to σ_θ is equal to

$$-\int_0^b 2\sigma_\theta h \sin\frac{\Delta\theta}{2}\frac{d(r+u)}{dr}\,dr$$

The centrifugal force on the same sector is equal to

$$\int_0^b \rho h_{init}\, r(\Delta\theta)\,\omega^2\,(r+u)\,dr$$

From the condition of equilibrium of the sector in the radial direction, the following equation is obtained:

$$\int_0^b \sigma_\theta h\frac{d(r+u)}{dr}\,dr = \int_0^b h_{init}\,\rho\omega^2\,(r+u)r\,dr$$

or

$$\rho(\omega b)^2 = \frac{\int_0^1 \sigma_\theta e^{-\epsilon_\theta}\,d\left(\frac{r}{b}\right)}{\int_0^1 \left(\frac{r}{b}\right)^2 e^{\epsilon_\theta}\,d\left(\frac{r}{b}\right)} \qquad (15)$$

The value of $\rho(\omega b)^2$ is then determined only by the tangential stress and strain. Accurate values of $\rho(\omega b)^2$ can be obtained by substituting into equation (15) the tangential stress and strain, σ_θ and ϵ_θ, calculated from the linearized solution.

APPROXIMATE VALUE OF ROTATING SPEED OF DISK DETERMINED DIRECTLY FROM TENSILE STRESS-STRAIN CURVE OF MATERIAL

If only the approximate value of the rotating-speed function $\rho(\omega b)^2$ is required, equation (15) can be made even simpler. Consider first the denominator because it is a function of ϵ_θ and r/b only. Expanding e^{ϵ_θ} into a series, the denominator becomes

$$\int_0^1 e^{\epsilon_\theta}\left(\frac{r}{b}\right)^2 d\left(\frac{r}{b}\right) = \int_0^1 \left[1 + \left(\frac{\epsilon_\theta}{\gamma}\right)\left(\frac{\gamma}{\gamma_o}\right)\gamma_o + \frac{1}{2!}\left(\frac{\epsilon_\theta}{\gamma}\right)^2\left(\frac{\gamma}{\gamma_o}\right)^2\gamma_o^2 + \cdots\right]\left(\frac{r}{b}\right)^2 d\left(\frac{r}{b}\right)$$

where γ_o is a constant and can be taken out of the integral sign. Thus the denominator of equation (15) becomes

$$\int_0^1 e^{\epsilon_\theta}\left(\frac{r}{b}\right)^2 d\left(\frac{r}{b}\right) = \frac{1}{3} + G_1\gamma_o + G_2\gamma_o^2 + \cdots \qquad (16a)$$

where G_1, G_2, and so forth are integrals, which are functions of α, γ/γ_o, and r/b only. The integrals are given in table I.

The integrals can be calculated using the values of α and γ/γ_o along r/b obtained from the approximate solution. The variations of α and γ/γ_o with r/b are independent of material according to the approximate solution.

The numerator of equation (15) is a function of σ_θ, ϵ_θ, and r/b. The tangential strain ϵ_θ can be treated in a manner similar to that used for the denominator. The tangential stress σ_θ can be written as $(\sigma_\theta/\tau)\tau$, where σ_θ/τ is a function of α, and τ can be written as an approximate function of γ; thus

$$\sigma_\theta = \left(\frac{\sigma_\theta}{\tau}\right)\tau = \left(\frac{\sigma_\theta}{\tau}\right) K\gamma^m$$

where m is the slope of a straight line approximating the tensile $\tau(\gamma)$ curve of the material on the logarithmic plot within the range of γ encountered along the radius of the disk γ_b to γ_o, and K is a constant that can be determined from the actual $\tau(\gamma)$ curve within the same range of γ. The integrand of the numerator thus becomes:

$$\sigma_\theta e^{-\epsilon_\theta} = K\gamma_o^m\left(\frac{\sigma_\theta}{\tau}\right)\left(\frac{\gamma}{\gamma_o}\right)^m e^{-\epsilon_\theta} = \tau_o\left(\frac{\sigma_\theta}{\tau}\right) e^{-\left(m \log_e \frac{\gamma_o}{\gamma} + \epsilon_\theta\right)}$$

Expanding the exponential function of e into a series gives

$$e^{-\left(m \log_e \frac{r_o}{r} + \epsilon_\theta\right)}$$

$$= 1 - \left(m \log_e \frac{r_o}{r} + \epsilon_\theta\right) + \frac{1}{2!}\left(m \log_e \frac{r_o}{r} + \epsilon_\theta\right)^2 - \frac{1}{3!}\left(m \log_e \frac{r_o}{r} + \epsilon_\theta\right)^3 + \cdots$$

$$= 1 - m \log_e \frac{r_o}{r} + \frac{m^2}{2!}\left(\log_e \frac{r_o}{r}\right)^2 - \frac{m^3}{3!}\left(\log_e \frac{r_o}{r}\right)^3 + \cdots$$

$$- \frac{\epsilon_\theta}{r}\frac{r}{r_o} r_o + m r_o \frac{\epsilon_\theta}{r}\frac{r}{r_o} \log_e \frac{r_o}{r} - \frac{m^2}{2!} r_o \frac{\epsilon_\theta}{r}\frac{r}{r_o}\left(\log_e \frac{r_o}{r}\right)^2 + \cdots$$

$$+ \frac{r_o^2}{2!}\left(\frac{\epsilon_\theta}{r}\right)^2\left(\frac{r}{r_o}\right)^2 - \frac{m r_o^2}{2!}\left(\frac{\epsilon_\theta}{r}\right)^2\left(\frac{r}{r_o}\right)^2 \left(\log_e \frac{r_o}{r}\right) + \cdots$$

$$- \frac{r_o^3}{3!}\left(\frac{\epsilon_\theta}{r}\right)^3\left(\frac{r}{r_o}\right)^3 + \cdots$$

The values of m and r_o remain constant along the radius and can therefore be taken out of the integral sign; thus the numerator of equation (15) becomes

$$\int_0^1 \sigma_\theta e^{-\epsilon_\theta} \, d\left(\frac{r}{b}\right) = \tau_o(I_0 - I_1 m + I_2 m^2 - I_3 m^3 + \cdots - I_4 r_o + I_5 m r_o + \cdots) \qquad (16b)$$

The integrals I_0, I_1, I_2, I_3, I_4, I_5, and so forth are functions of α, r/r_o, and r/b, and are independent of material according to the approximate solution. These integrals are also given in table I. Substituting equations (16a) and (16b) into equation (15) and neglecting the small terms result in

$$\frac{\rho(\omega b)^2}{\tau_o} = \frac{I_0 - I_1 m + I_2 m^2 - I_3 m^3 - I_4 r_o + I_5 m r_o}{\frac{1}{3} + G_1 r_o + G_2 r_o^2} \qquad (17)$$

The values of I_0, I_1, . . . G_1, and G_2 are calculated from the formulas listed in table I by using the α, γ/γ_o, and r/b relations obtained in the case of $n = 0$ (the approximate solution). These values are as follows:

I_0	2.3031	I_4	0.5239
I_1	2.0281	I_5	.3514
I_2	1.3131	G_1	.0537
I_3	.6362	G_2	.0047

Equation (17) shows that $\rho(\omega b)^2/\tau_o$ is a function of m and γ_o. The value of γ_o is the maximum value of γ in the disk. Once the value of γ_o is selected, m can be obtained from the tensile $\tau(\gamma)$ curve of the material within the range of γ considered (γ_b to γ_o, γ_b/γ_o is approximately equal to 0.15), and τ_o is the value of τ corresponding to γ_o taken from the $\tau(\gamma)$ curve of the material. Equation (17) thus gives the approximate value of $\rho(\omega b)^2$, which is directly determined from the tensile stress-strain curve of the material. Curves of $\rho(\omega b)^2/\tau_o$ against γ_o for different constant values of m can be calculated and plotted. The value of $\rho(\omega b)^2/\tau_o$ can then be read directly from the chart for given values of m and γ_o.

CORRELATION BETWEEN EXPERIMENTAL BURSTING SPEED AND CALCULATED VALUE DETERMINED DIRECTLY FROM TENSILE STRESS-STRAIN CURVE OF MATERIAL

It is interesting to compare the experimentally determined rotating speed corresponding to a value of γ_o at the center of the disk with the rotating speed predicted from the chart (or equation (17)) mentioned in the previous section. In order to determine these speeds experimentally, it would be necessary to measure γ_o at the centers of the rotating disks during operation. Such data are unavailable in the literature to the best knowledge of the author. If it is assumed that fracture in the rotating disk takes place at the same value of γ_o as the fracture octahedral shear strain in simple tension, then the data in reference 4,

together with additional data obtained at the Lewis laboratory for the work reported in reference 4, are sufficient to allow comparison between prediction and experiment.

The predicted rotating speed is determined directly from the tensile octahedral shear stress-strain curve of the same material as the disk. These curves are calculated from the unpublished tensile test data for reference 4. The tensile specimens were cut in the radial direction of the disk of the same material and same heat treatment. The specimen was 3.00 inches long with a 1.00-inch gage length. Detailed dimensions of the tensile specimen are given in figure 4 of reference 4. During the tensile test, the load-elongation curve was obtained by a recording extensiometer. The original and breaking diameters of specimens were measured before and after the experiment. The load at which the specimen broke was read from the dial of the tensile machine. From these data, a $\tau(\gamma)$ curve of the material can be obtained. First, calculate τ and γ by using the values taken from the load-elongation curve up to the maximum load point:

$$\gamma = \sqrt{2}\,\epsilon_1 = \sqrt{2}\,\log_e(1+\Delta l)$$

$$\tau = \frac{\sqrt{2}}{3}\sigma_1 = \frac{\sqrt{2}}{3}\frac{P}{A} = \frac{\sqrt{2}}{3}\frac{P}{A_o}\frac{A_o}{A} = \frac{\sqrt{2}}{3}\frac{P}{A_o}(1+\Delta l) \qquad (18)$$

where

Δl elongation of 1-inch gage length

A instantaneous area

A_o original area

l instantaneous length

l_o original length

P load of tensile specimen

The τ and γ relation cannot be obtained from the tensile load-elongation curve after the maximum load is reached because of the nonuniform elongation within the gage length. However, the τ and γ at fracture can be calculated from the original cross-sectional area, fracture area, and fracture load:

$$\left.\begin{aligned} \tau_{fr} &= \frac{\sqrt{2}}{3}\frac{P_{fr}}{A_{fr}} \\ \gamma_{fr} &= \sqrt{2}\log_e \frac{A_o}{A_{fr}} \end{aligned}\right\} \qquad (18a)$$

where the subscript fr means at fracture. Plot the τ and γ relation obtained on a logarithmic scale. Draw a straight line to approximate the $\tau(\gamma)$ curve in the range of $\gamma_{fr}(\gamma_b/\gamma_o)$ to γ_{fr}; for a solid rotating disk, γ_b/γ_o is approximately equal to 0.15 (for the case of $n = 0$). The slope of this straight line gives the value of m. Find the value of $\rho(\omega b)^2/\tau_o$ corresponding to m and $\gamma_o = \gamma_{fr}$ from the chart. The predicted value of $\rho(\omega b)^2$ when the disk bursts will be equal to $\left[\rho(\omega b)^2/\tau_o\right]\tau_{fr}$ by assuming the disk breaks when the maximum γ in the disk (γ_o at the center of the disk) reaches the value of γ_{fr} in simple tension.

2125

CALCULATIONS, RESULTS, AND DISCUSSION

In order to observe the degree of the approximation resulting from the use of a power function representing the octahedral shear stress-strain relation over the complete strain-hardening range (power-law approximation), a calculation is made with the following relation between τ and γ:

$$\tau(\gamma) = 126{,}000\ \gamma^{0.25}$$

The constants are chosen to approximate the $\tau(\gamma)$ curve of Inconel X over the whole strain-hardening range, as shown in figure 2. In figure 3, the variations of α, γ, σ_r, σ_θ, ϵ_r, and ϵ_θ with r/b for the case of $\gamma_o = 0.30$ obtained by the power-law approximation are compared with the values obtained from the actual $\tau(\gamma)$ curve of Inconel X; it can be seen that the power-law approximation gives good results. These results indicate that replacing the term $\frac{\gamma}{\tau}\frac{d\tau}{d\gamma}$ in equations (9b) by m should introduce very little error. Also, if a simple analytical function of $\tau(\gamma)$ is desired for analysis, the simple power function representing the τ and γ relation of a given material will give a very good approximation.

The values of α and γ/γ_o along the radius are calculated for $n = -0.05$, 0, 0.1, 0.2, and 0.3 from the partly linearized equations (13). The variations of α and γ/γ_o with r/b for the different values of n are plotted in figure 4; these values are given in table II. The values of α and γ/γ_o along r/b obtained in reference 5 for 16-25-6 and Inconel X are plotted in figure 5; the values of n for these cases are calculated from equation (12a) and indicated on these curves. The curves obtained from the partly linearized solution in figure 4 having the same range of values of n as those obtained from reference 5 are also plotted in figure 5 for comparison. The curves for the same n value of the two solutions agree very well for most cases. For simplicity, the solution based on the deformation theory obtained in reference 5 is designated the exact solution. The simple relation $n = m - 0.5\,\gamma_o$ can then be used as a good approximate criterion to find the variation of α and γ/γ_o with r/b for different materials and different maximum strains. This generality leads to a general criterion of applicability of the deformation theory of plasticity to this problem for any material in the strain-hardening range. The criterion is that if the value of n for a given material is constant or approximately constant in the strain-hardening range, the deformation theory can be applied to this problem for the material. For the special case of infinitesimal strain, the condition of n being constant reduces to m being constant, which is the same condition obtained by Ilyushin (reference 11).

In figure 4(a), the maximum variation of α is about 15 percent whereas n varies from -0.05 to 0.3. For most materials, m increases with γ; thus it can be seen from equation (12a) that m and γ affect n in an opposite sense, so that n does not change much with strain. The value of n for most materials of any maximum strain γ_o varies from -0.05 to 0.3 (references 12 to 14); only a small part of this variation is due to the variation with strain for a given material. The variation of α during loading is expected to be very small for most materials; consequently the deformation theory of plasticity is applicable to this problem within engineering accuracy.

The values of σ_r/τ, σ_θ/τ, ϵ_r/γ, and ϵ_θ/γ are calculated from equations (7a) and (8a) for the range of α considered and are given in table III. The distributions of principal stresses and strains are obtained by the partly linearized solution for the

cases of $\gamma_o = 0.3000$ for Inconel X and $\gamma_o = 0.4400$ for 16-25-6. These results are plotted in figure 6. The results obtained by the exact solution are also plotted for comparison. The examples with $\gamma_o = 0.3000$ for Inconel X and $\gamma_o = 0.4400$ for 16-25-6, with the values of n equal to 0.15 and -0.05, respectively, are chosen because they give the largest deviation of the examples considered between the partly linearized and exact solutions in curves of α and γ/γ_o against r/b. For $\gamma_o = 0.3000$, Inconel X, n is equal to 0.15 and the values of α and γ/γ_o corresponding to different values of r/b can be obtained from table I by linear interpolation. In figure 6, the principal stress and strain distributions obtained by the partly linearized solution are shown to agree very well with those obtained by the exact solution, even for these two cases that have the largest deviation of the variations of α and γ/γ_o with r/b between the two solutions. For the rest of the cases, the α and γ/γ_o curves obtained by the two solutions are approximately the same; therefore the distributions of principal stresses and strains will also be practically the same.

The variations of α and γ/γ_o with r/b obtained by the approximate solution are the same as those for the case of $n = 0$ in figure 4. The principal strains obtained by the approximate solution and the exact solution are plotted in figures 7(a) and 7(b) for 16-25-6 and Inconel X, respectively. The stress distributions obtained by these two solutions are plotted in figures 7(c) and 7(d) for 16-25-6 and Inconel X, respectively. The stresses and the strains obtained by the approximate solution give fairly good results.

The variations of α, γ/γ_o, $\epsilon_\theta/(\epsilon_\theta)_o$, and $\epsilon_r/(\epsilon_r)_o$ with radius for ideally plastic material are the same as those obtained by the approximate method. The principal stresses for the ideally plastic material with γ_o equal to 0.4400 and 0.3000 are also calculated. In this case, τ is constant and is chosen equal to the τ_o for which the solutions are being compared. These distributions of principal stresses along the radius as well as those obtained by the partly linearized, exact, and approximate solutions are plotted in figures 8(a) and 8(b) for the case of $\gamma_o = 0.4400$ for 16-25-6, and $\gamma_o = 0.3000$ for Inconel X, respectively, for comparison. It is seen from these figures that the stresses (especially the tangential stress, which is the most important part of the solution) obtained by the ideally plastic material are not good

enough to represent the actual results. The curves obtained by the three other methods agree very well. These results also indicate, as in the case of the thin plate with a circular hole (reference 6) that the ratios of strains along the radius to the maximum value and the ratio of the principal stresses are essentially independent of the $\tau(\gamma)$ curve of the material and the maximum strain of the disk, but that the stresses are very much dependent on the material. The conclusions obtained in reference 5 for the problem of the rotating disk (with body force) of Inconel X and 16-25-6 are then extended to most materials.

The rotating-speed function $\rho(\omega b)^2$ is calculated from equation (15) by using the values of σ_θ and ϵ_θ obtained in the partly linearized solution for Inconel X and 16-25-6. These values of $\rho(\omega b)^2$ and those obtained from the exact solution are plotted against γ_o in figure 9. The loads obtained by these two methods are practically the same (the two curves coincide). The relations between the approximate value of $\rho(\omega b)^2/\tau_o$ and γ_o for several values of m are calculated from equation (17) and plotted in figure 10. The variations of load $\rho(\omega b)^2$ with γ_o for Inconel X and 16-25-6 are obtained from figure 10 and are plotted in figure 9 for comparison. The values obtained by the approximate solution are also very close to the values obtained by the exact solution. The percentage deviation of $\rho(\omega b)^2$ of the approximate solution from the exact solution is much less than the percentage deviation of tangential stress and strain. This can be explained by the fact that $\rho(\omega b)^2$ (equation (15)) increases with increasing value of σ_θ but decreases with increasing value of ϵ_θ; values of σ_θ and ϵ_θ obtained by the approximate solution (fig. 7) differ from those of the exact solution in the same direction; hence the part of error cancels. The percentage deviations of radial stress and strain in some cases are quite large, but fortunately these quantities do not enter in the calculation of $\rho(\omega b)^2$.

Use is made of figure 10 to calculate $\rho(\omega b)^2$ from the tensile stress-strain curve of the same materials as the solid disks considered in reference 4. (In this reference, data were obtained for disks that showed no imperfections upon X-ray and surface inspection and for disks in which defects did exist. For the present purposes, only the disks having no defects were considered.) From the load-elongation curve, original diameter, final diameter, and fracture load in tension, which data were obtained at this laboratory for the work reported in reference 4, the $\tau(\gamma)$ curves of

these materials were calculated using equations (18) and (18a) and are plotted in figure 11 on a logarithmic scale. Six materials (SAE 1078 steel of two different heat treatments, beryllium-copper alloy of three different heat treatments, and one nickel-base alloy) are considered. For simplicity, these materials are herein designated materials A, B, C, D, E, and F. The values of τ_{fr} and γ_{fr} for these materials are given in table IV; the reduction in nonnecked diameter, which was used as a parameter in some figures of reference 4, is also given in table IV in order to correlate the results given in reference 4 and herein. (This reduction in nonnecked diameter is the reduction in diameter in the region of uniform strain of the specimen.) In table IV are listed the values of m and $\rho(\omega b)^2$, which are calculated by taking γ_o at the center of the disk equal to γ_{fr} of the tensile test, except for material C. Because the load-elongation curves of the tensile test show that material C has a large necking effect, several values of $\rho(\omega b)^2$ for different γ_o between $\gamma = 0.1342$ (the γ at the maximum load of the tensile test) and γ_{fr} were calculated and are given in table V. It can be seen that the calculated rotating-speed function $\rho(\omega b)^2$ increases to a maximum at $\gamma_o = 0.3$ to 0.4 and then decreases. This fact indicates a case of instability of the rotating disk.

The experimentally determined values of $\rho(\omega b)^2$ are also given in table IV. The percentage difference of calculated $\rho(\omega b)^2$ to the experimentally determined $\rho(\omega b)^2$ as well as the percentage difference of calculated ω to the experimentally determined ω is given in the same table. It can be seen from these values that the percentage difference in ω is small. More reliable calculated values of $\rho(\omega b)^2$ may be obtained, however, if: (1) the $\tau(\gamma)$ curves obtained from the tensile test are corrected for the triaxiality and nonuniform stress distribution introduced by necking, and (2) the $\tau(\gamma)$ curve of a few tangential tensile specimens taken at different radii of the disk (including a specimen passing through the center of the disk) are used, because the material of the disk is not quite uniform and $\rho(\omega b)^2$ is a function of ϵ_θ, σ_θ, and r/b, as shown in equation (15). The calculated values of $\rho(\omega b)^2$ at disk failure are plotted against the experimentally determined $\rho(\omega b)^2$ in figure 12. It can be seen that these points are slightly above the 45° straight line. Calculations based on $\tau(\gamma)$ curves of tangential tensile specimens may give lower values.

It should be emphasized that all the results and discussion are only true for this problem under plastic deformation in the strain-hardening range in which the elastic strains are small compared with the plastic strains and there are neither time and temperature effects nor unloading.

CONCLUSIONS

The results obtained for the rotating disk in the strain-hardening range, in which the elastic strains are small compared with the plastic strains, lead to the following conclusions, which are similar to those obtained in the case of the thin plate with a circular hole:

1. The results obtained by the partly linearized solution agree very well with those obtained by the exact solution based on the deformation theory of plasticity. The amount of computation is greatly reduced by the partial linearization. The stresses and the strains can be obtained for any material under any maximum strain by a simple multiplication using the tables or curves given in this paper.

2. The variation of a parameter, which is determined from the tensile-stress-and-strain curve of the material, can be used as a simple general criterion of the applicability of deformation theory for this problem.

3. The results previously obtained for Inconel X and 16-25-6, namely, the variation of the ratio of the principal stresses with radius and the ratios of the strain along the radius to their maximum value are essentially independent of the octahedral shear stress-strain relation of the material but that the distributions of the stresses depend very much on the material, are extended to most materials.

4. Results obtained for the ideally plastic material with the infinitesimal strain concept give good approximate values of principal strains but not principal stresses.

5. Sufficiently accurate values of principal stresses can be obtained by an approximate method in which the stresses are calculated by using the strains obtained from the ideally plastic material together with the actual octahedral shear stress-strain relation of the material.

6. The rotating speeds of the disk obtained by the partly linearized solution are practically the same as those obtained by the exact solution; and those obtained by the approximate solution, in which the rotating speeds are determined directly from the tensile stress-strain curve of the material, are also very close to the exact value.

7. Good correlation between experimental bursting speed and the calculated value determined directly from the tensile stress-strain curve of the material is obtained.

8. If a simple analytical function representing the octahedral shear stress-strain relation is required for analysis, the power-law approximation can be used.

Lewis Flight Propulsion Laboratory,
National Advisory Committee for Aeronautics,
Cleveland, Ohio, January 23, 1951.

REFERENCES

1. Nadai, A., and Donnell, L. H.: Stress Distribution in Rotating Disks of Ductile Material after the Yield Point has been Reached. APM-51-16, Trans. A.S.M.E., vol. 51, pt. 1, 1929, pp. 173-180; discussion, pp. 180-181.

2. Millenson, M. B., and Manson, S. S.: Determination of Stresses in Gas-Turbine Disks Subjected to Plastic Flow and Creep. NACA Rep. 906, 1948. (Formerly NACA TN 1636.)

3. MacGregor, C. W., and Tierney, W. D.: Developments in High-Speed Rotating Disk Research at M.I.T. Welding Jour. Suppl., vol. 27, no. 6, June 1948, pp. 303S-309S.

4. Holms, Arthur G., and Jenkins, Joseph E.: Effect of Strength and Ductility on Burst Characteristics of Rotating Disks. NACA TN 1667, 1948.

5. Wu, M. H. Lee: Analysis of Plane-Stress Problems with Axial Symmetry in Strain-Hardening Range. NACA TN 2217, 1950.

6. Wu, M. H. Lee: Linearized Solution and General Plastic Behavior of Thin Plate with Circular Hole in Strain-Hardening Range. NACA TN 2301, 1951.

7. Nádai, A.: Plasticity. McGraw-Hill Book Co., Inc., 1931.

8. Nadai, A.: Plastic Behavior of Metals in the Strain-Hardening Range. Part I. Jour. Appl. Phys., vol. 8, no. 3, March 1937, pp. 205-213.

9. Davis, Evan A.: Plastic Behavior of Metals in the Strain Hardening Range. Part II. Jour. Appl. Phys., vol. 8, no. 3, March 1937, pp. 213-217.

10. MacGregor, C. W.: Relations between Stress and Reduction in Area for Tensile Test of Metals. T.P. 805, Metals Tech., vol. 4, no. 3, April 1937, pp. 1-19.

11. Ilyushin, A. A.: The Theory for Small Elastic-Plastic Deformations. RMB-17, trans. by Grad. Div. Appl. Math., Brown Univ., for David W. Taylor Model Basin (Washington, D.C.), 1947. (Contract NObs-34166.)

12. MacGregor, C. W.: The Tension Test. Proc. A.S.T.M., vol. 40, 1940, pp. 508-534.

13. Low, John R., Jr., and Garofalo, Frank: Precision Determination of Stress-Strain Curves in the Plastic Range. Proc. Soc. Exper. Stress Analysis, vol. 4, no. 2, 1947, p. 16.

14. Hollomon, John H.: Tensile Deformation. Trans. A.I.M.E., Iron and Steel Div., vol. 162, 1945, pp. 268-289.

TABLE I - VALUES OF I AND G USED IN EQUATIONS (16) AND (17)

$$I_0 = \int_0^1 \left(\frac{\sigma_\theta}{\tau}\right) d\left(\frac{r}{b}\right) = 2.3031$$

$$I_1 = \int_0^1 \left(\frac{\sigma_\theta}{\tau}\right) \log_e \frac{r_o}{r} \, d\left(\frac{r}{b}\right) = 2.0281$$

$$I_2 = \frac{1}{2} \int_0^1 \left(\frac{\sigma_\theta}{\tau}\right) \left(\log_e \frac{r_o}{r}\right)^2 d\left(\frac{r}{b}\right) = 1.3131$$

$$I_3 = \frac{1}{6} \int_0^1 \left(\frac{\sigma_\theta}{\tau}\right) \left(\log_e \frac{r_o}{r}\right)^3 d\left(\frac{r}{b}\right) = 0.6362$$

$$I_4 = \int_0^1 \left(\frac{\sigma_\theta}{\tau}\right)\left(\frac{\epsilon_\theta}{r}\right)\left(\frac{r}{r_o}\right) d\left(\frac{r}{b}\right) = 0.5239$$

$$I_5 = \int_0^1 \left(\frac{\sigma_\theta}{\tau}\right)\left(\frac{\epsilon_\theta}{r}\right)\left(\frac{r}{r_o}\right) \log_e \frac{r_o}{r} \, d\left(\frac{r}{b}\right) = 0.3514$$

$$G_1 = \int_0^1 \left(\frac{\epsilon_\theta}{r}\right)\left(\frac{r}{r_o}\right)\left(\frac{r}{b}\right)^2 d\left(\frac{r}{b}\right) = 0.0537$$

$$G_2 = \frac{1}{2} \int_0^1 \left(\frac{\epsilon_\theta}{r}\right)^2 \left(\frac{r}{r_o}\right)^2 \left(\frac{r}{b}\right)^2 d\left(\frac{r}{b}\right) = 0.0047$$

TABLE II - VARIATION OF α AND r/r_o WITH r/b

FOR VARIOUS VALUES OF n

α	$n = -0.05$		$n = 0$		$n = 0.1$		$n = 0.2$		$n = 0.3$	
	r/b	r/r_o	r/b	r/r_o	r/b	r/r_o	r/b	r/r_o	r/b	r/r_o
1.5708	0.0000	1.0000	0.0000	1.0000	0.0000	1.0000	0.0000	1.0000	0.0000	1.0000
1.5675	.0480	.9850	.0510	.9850	.0600	.9850	.0690	.9850	.0800	.9850
1.5615	.0750	.9675	.0900	.9675	.1010	.9675	.1140	.9675	.1260	.9675
1.5480	.1170	.9250	.1325	.9250	.1565	.9250	.1780	.9250	.2050	.9250
1.5300	.1555	.8700	.1780	.8710	.2050	.8730	.2350	.8750	.2720	.8770
1.5045	.2025	.8010	.2250	.8030	.2580	.8060	.2970	.8090	.3380	.8120
1.4820	.2370	.7490	.2600	.7500	.2970	.7550	.3400	.7590	.3840	.7630
1.4490	.2820	.6780	.3050	.6820	.3475	.6880	.3930	.6920	.4400	.6960
1.4105	.3280	.6100	.3510	.6150	.3975	.6210	.4420	.6280	.4910	.6350
1.3670	.3775	.5420	.4000	.5490	.4460	.5580	.4920	.5675	.5410	.5760
1.3180	.4280	.4790	.4505	.4875	.4950	.4995	.5400	.5120	.5900	.5210
1.2635	.4820	.4200	.5025	.4295	.5450	.4450	.5890	.4575	.6370	.4710
1.2045	.5350	.3690	.5540	.3790	.5940	.3950	.6360	.4120	.6800	.4250
1.1400	.5880	.3230	.6060	.3345	.6440	.3520	.6830	.3695	.7230	.3850
1.0705	.6440	.2840	.6600	.2950	.6930	.3145	.7290	.3325	.7650	.3500
.9965	.7000	.2505	.7150	.2610	.7440	.2820	.7730	.3000	.8050	.3175
.9175	.7575	.2220	.7700	.2330	.7930	.2525	.8170	.2720	.8440	.2915
.8330	.8140	.1975	.8240	.2075	.8420	.2280	.8610	.2480	.8820	.2690
.7430	.8710	.1760	.8780	.1870	.8920	.2070	.9040	.2270	.9180	.2490
.6465	.9290	.1590	.9330	.1690	.9410	.1900	.9490	.2100	.9560	.2310
.5236	1.0000	.1430	1.0000	.1520	1.0000	.1720	1.0000	.1930	1.0000	.2150

TABLE III - VALUES OF σ_r/τ, σ_θ/τ, ϵ_r/γ, AND ϵ_θ/γ

FOR CORRESPONDING VALUE OF α

α	σ_r/τ	σ_θ/τ	ϵ_r/γ	ϵ_θ/γ
1.5708	2.1213	2.1213	0.3536	0.3536
1.5675	2.1172	2.1253	.3515	.3556
1.5615	2.1098	2.1326	.3478	.3592
1.5480	2.0929	2.1487	.3395	.3674
1.5300	2.0696	2.1695	.3283	.3782
1.5045	2.0355	2.1978	.3122	.3933
1.4820	2.0044	2.2216	.2979	.4065
1.4490	1.9568	2.2544	.2765	.4253
1.4105	1.8986	2.2896	.2513	.4468
1.3670	1.8295	2.3253	.2223	.4702
1.3180	1.7476	2.3602	.1892	.4955
1.2635	1.6515	2.3924	.1518	.5222
1.2045	1.5419	2.4192	.1108	.5494
1.1400	1.4160	2.4389	.0655	.5770
1.0705	1.2738	2.4488	.0165	.6040
.9965	1.1157	2.4463	-.0358	.6295
.9175	.9401	2.4289	-.0915	.6530
.8330	.7458	2.3935	-.1503	.6735
.7430	.5331	2.3370	-.2118	.6902
.6465	.3003	2.2555	-.2758	.7018
.5236	.0000	2.1213	-.3536	.7071

TABLE IV - DISK MATERIALS, TENSILE-TEST PROPERTIES, CALCULATED AND EXPERIMENTALLY DETERMINED BURST SPEEDS OF ROTATING DISK

Material[a]	Tensile-test properties				Burst speed				Difference of calculated to experimental $\rho(\omega b)^2$ (percent)	Difference of calculated to experimental ω (percent)
					Calculated from tensile $\tau(\gamma)$ curve			Experimentally determined $\rho(\omega b)^2$		
	Reduction in nonnecked diameter (percent)	τ_{fr}	γ_{fr}	m (in range of $\gamma_{fr}(\gamma_b/\gamma_o)$ to γ_{fr})	$\rho(\omega b)^2/\gamma_o$ from fig. 10	Calculated $\rho(\omega b)^2$	Average calculated $\rho(\omega b)^2$			
Steel, SAE 1078										
A	2.0	68,900	0.1237	0.186	5.61	386×10^3	382.5×10^3	381.5×10^3	0.26	0.13
		65,800	.0897	.170	5.77	379				
B	2.5	52,500	.1298	.155	5.75	301	309	289.1	6.54	3.22
		58,000	.2133	.173	5.47	317		292.8	5.19	2.56
Beryllium copper										
C	6.0	78,120	.8224	.192	4.15	324		310.2	4.51	2.16
D	9.0	78,300	1.3580	.413	2.72	212		206.2	2.81	1.40
E	16.9	76,000	1.3570	.480	2.60	197.5		191.4	3.19	1.57
Nickel-base alloy										
F	8.2	94,700	0.2957	.305	4.76	450	445	433.9	2.56	1.34
		89,500	.2338	.294	4.92	440		428.2	3.92	2.02

[a]Two different heat treatments for SAE 1078 and three different heat treatments for beryllium-copper alloy.

TABLE V - RELATION BETWEEN ROTATING SPEED $\rho(\omega b)^2$ AND MAXIMUM OCTAHEDRAL SHEAR STRAIN AT CENTER OF DISK FOR MATERIAL C (BERYLLIUM-COPPER)

γ_o	τ_o	m	$\rho(\omega b)^2/\tau_o$ from fig. 10	Calculated $\rho(\omega b)^2$
0.1342	54,560	0.092	6.04	330×10^3
.2000	58,000	.112	5.80	336
.3000	62,800	.152	5.38	337
.4000	66,200	.162	5.10	337
.5000	69,800	.185	4.81	336
.8224	78,120	.192	4.15	324

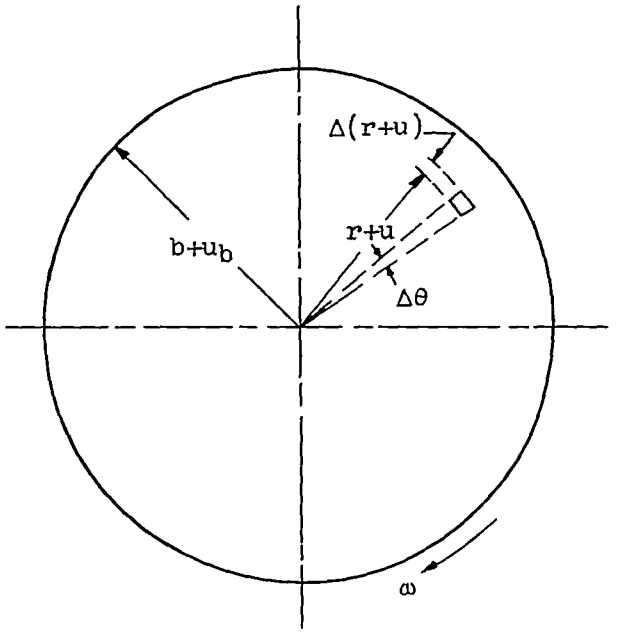

(a) Rotating disk.

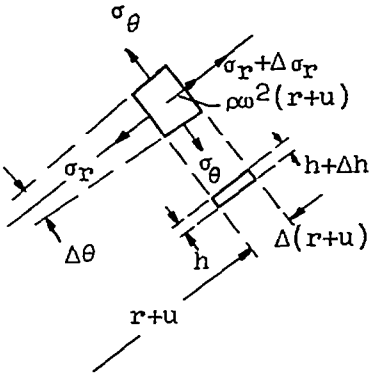

(b) Element.

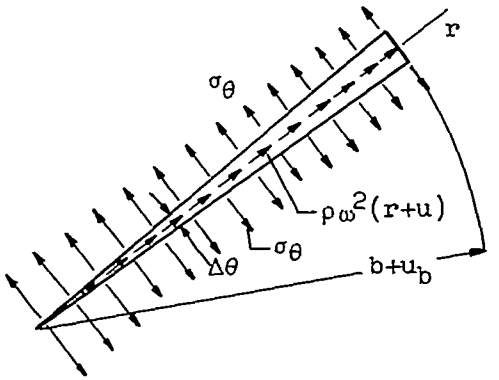

(c) Sector.

Figure 1. - Rotating disk, an element, and a sector in deformed state.

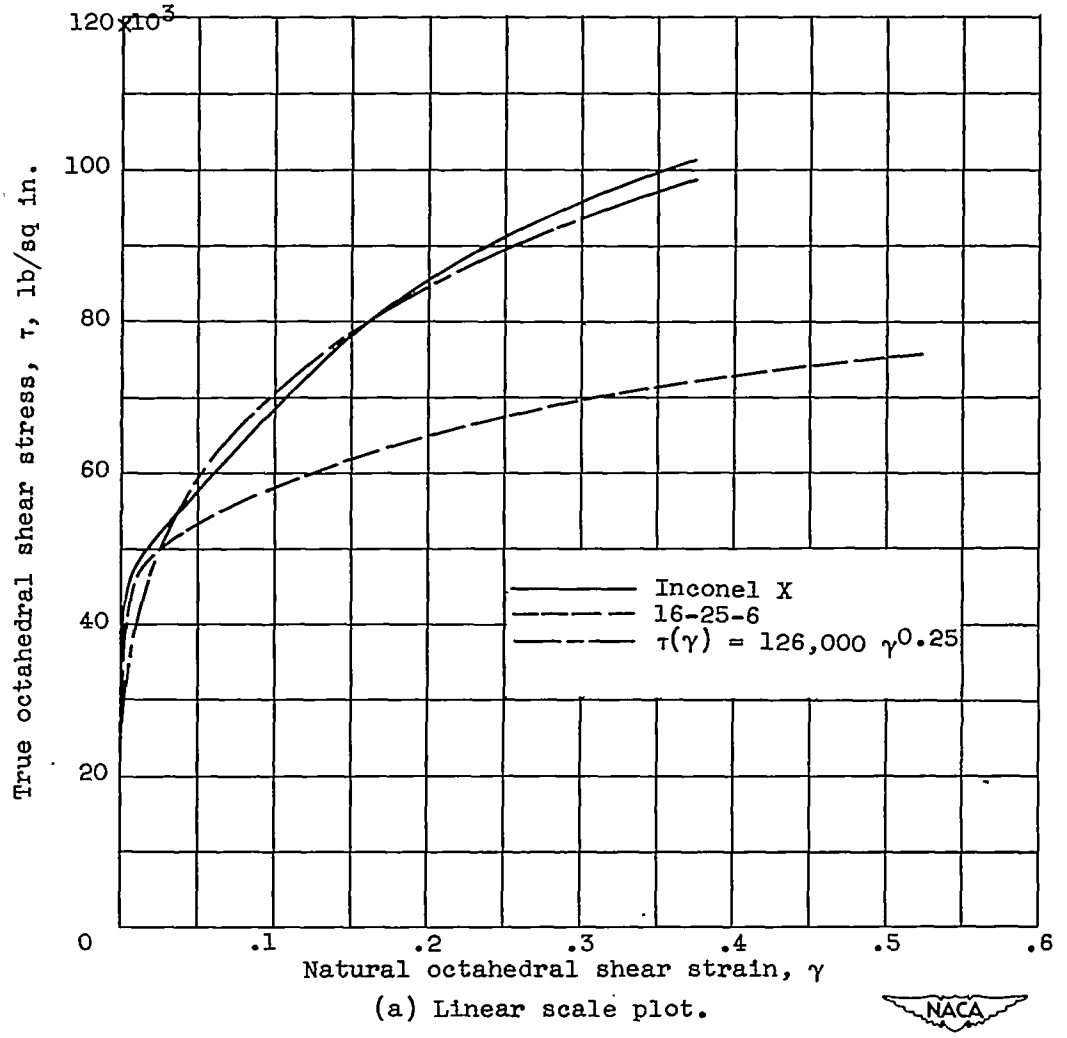

(a) Linear scale plot.

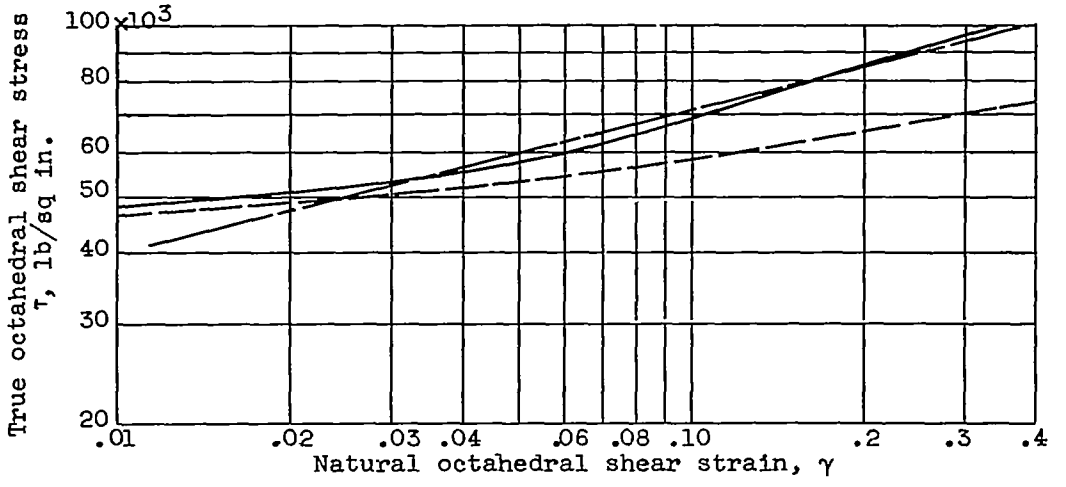

(b) Logrithmic scale plot.

Figure 2. - Octahedral shear stress-strain curves.

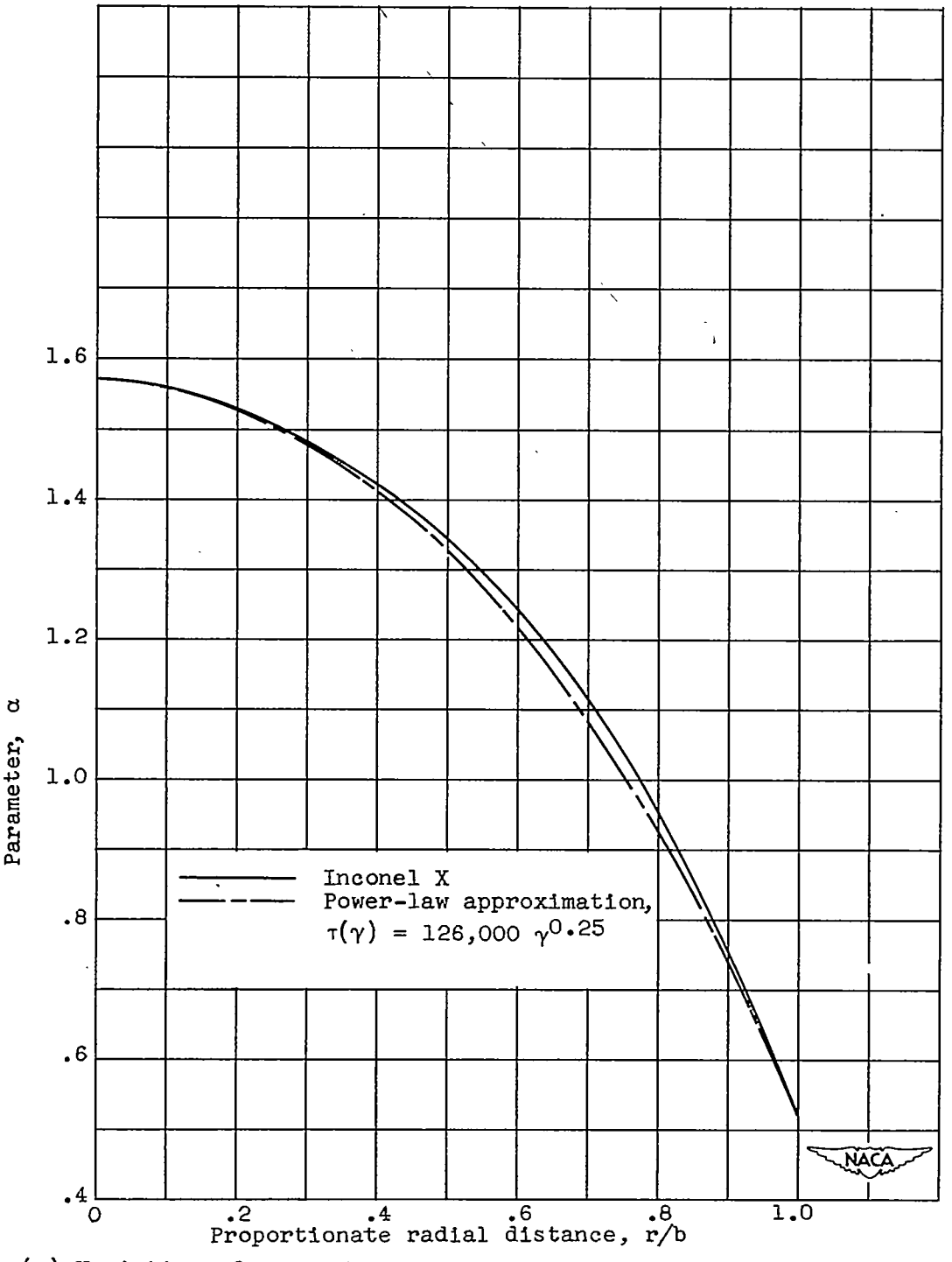

(a) Variation of parameter α with proportionate radial distance.

Figure 3. - Comparison of results obtained for $\tau(\gamma)$ for Inconel X and power-law approximation, $\tau(\gamma) = 126{,}000\ \gamma^{0.25}$ for rotating disk. $\gamma_o = 0.30$.

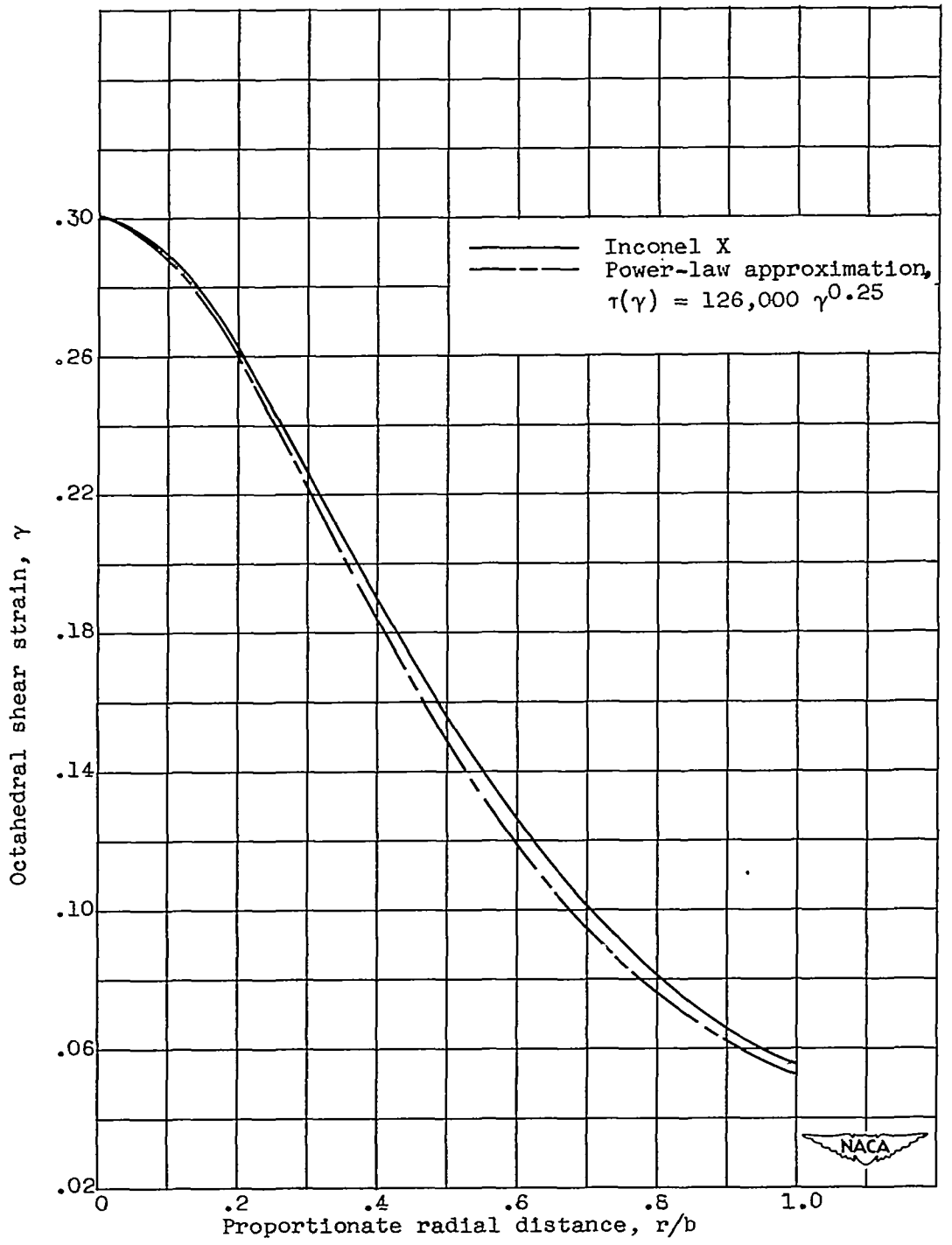

(b) Variation of octahedral shear strain with proportionate radial distance.

Figure 3. - Continued. Comparison of results obtained for $\tau(\gamma)$ for Inconel X and power-law approximation, $\tau(\gamma) = 126{,}000\ \gamma^{0.25}$ for rotating disk. $\gamma_o = 0.30$.

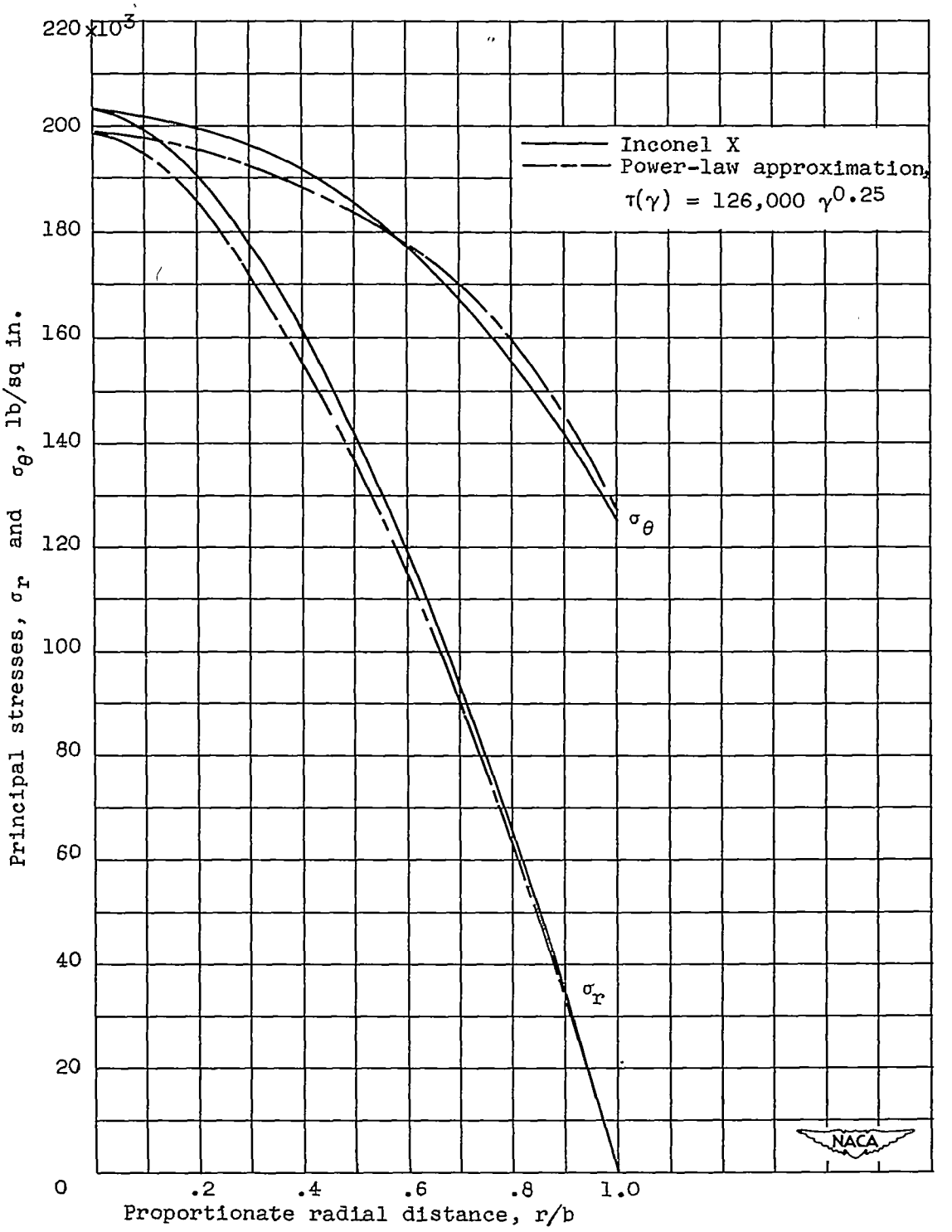

(c) Variation of principal stresses with proportionate radial distance.

Figure 3. - Continued. Comparison of results obtained for $\tau(\gamma)$ for Inconel X and power-law approximation, $\tau(\gamma) = 126{,}000\ \gamma^{0.25}$ for rotating disk. $\gamma_o = 0.30$.

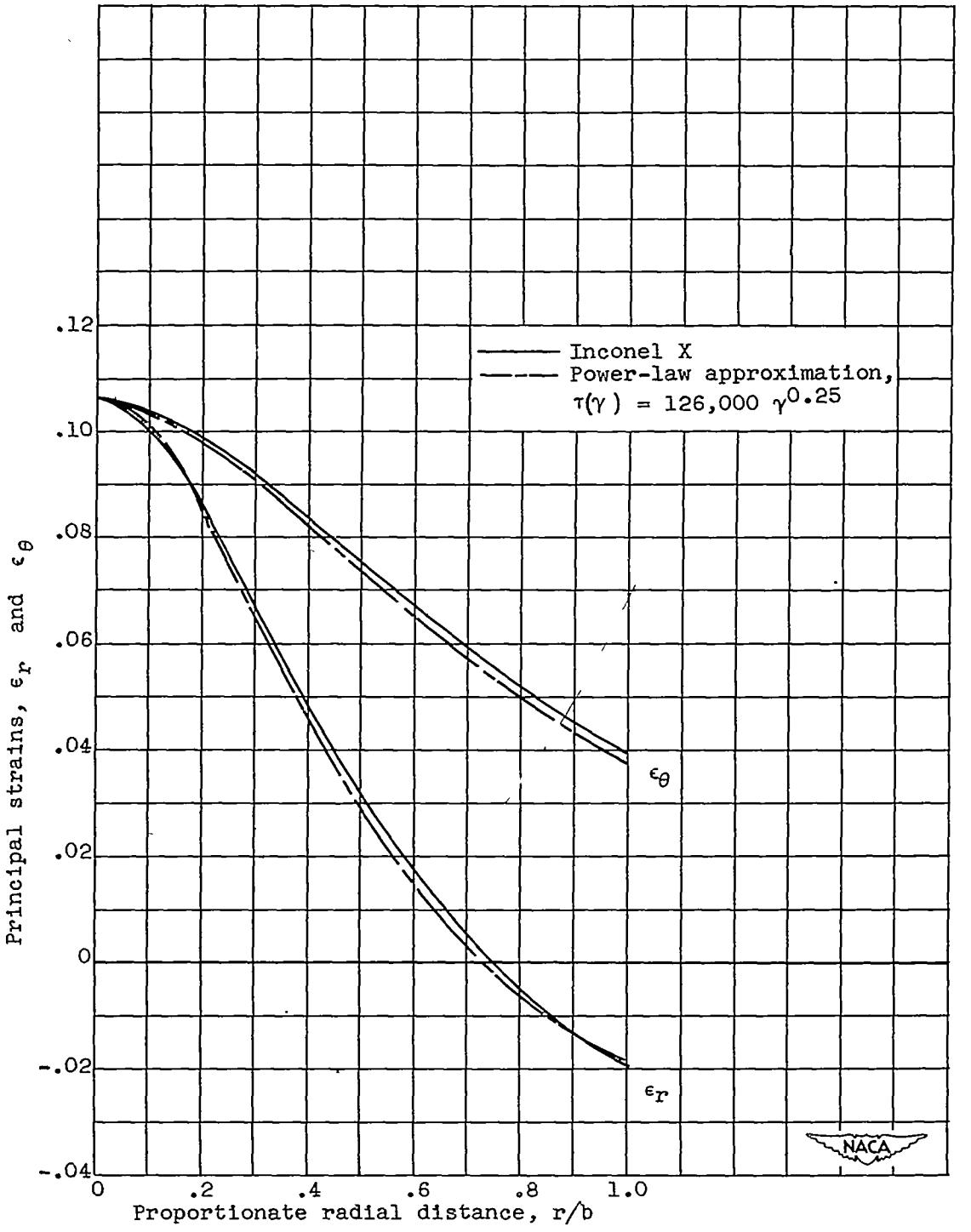

(d) Variation of principal strains with proportionate radial distance.

Figure 3. - Concluded. Comparison of results obtained for $\tau(\gamma)$ for Inconel X and power-law approximation, $\tau(\gamma) = 126{,}000\ \gamma^{0.25}$ for rotating disk. $\gamma_o = 0.30$.

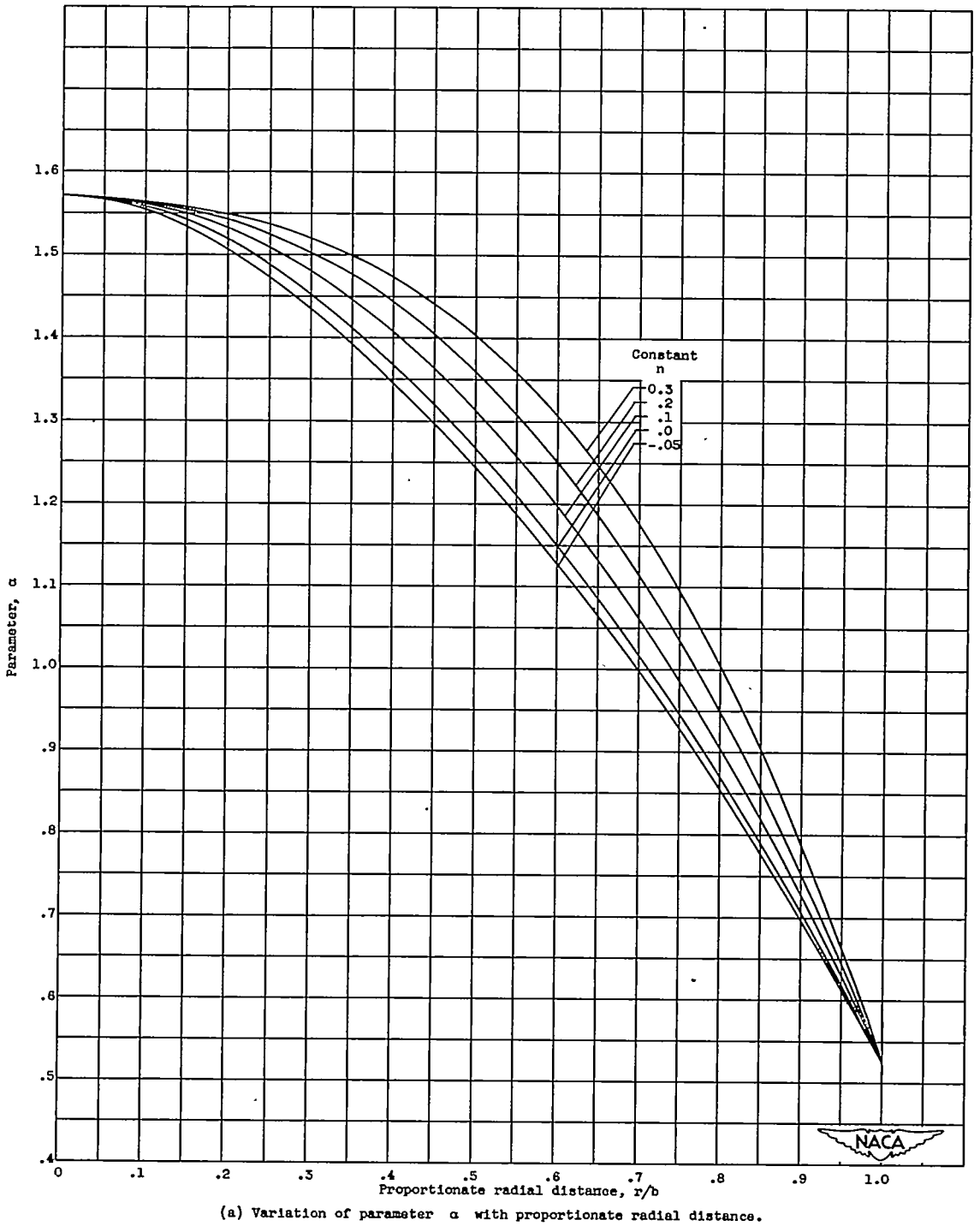

(a) Variation of parameter α with proportionate radial distance.

Figure 4. - Variations of parameter α and ratio of octahedral shear strain to octahedral shear strain at center γ/γ_o with proportionate radial distance r/b obtained by partly linearized solution for different values of n.

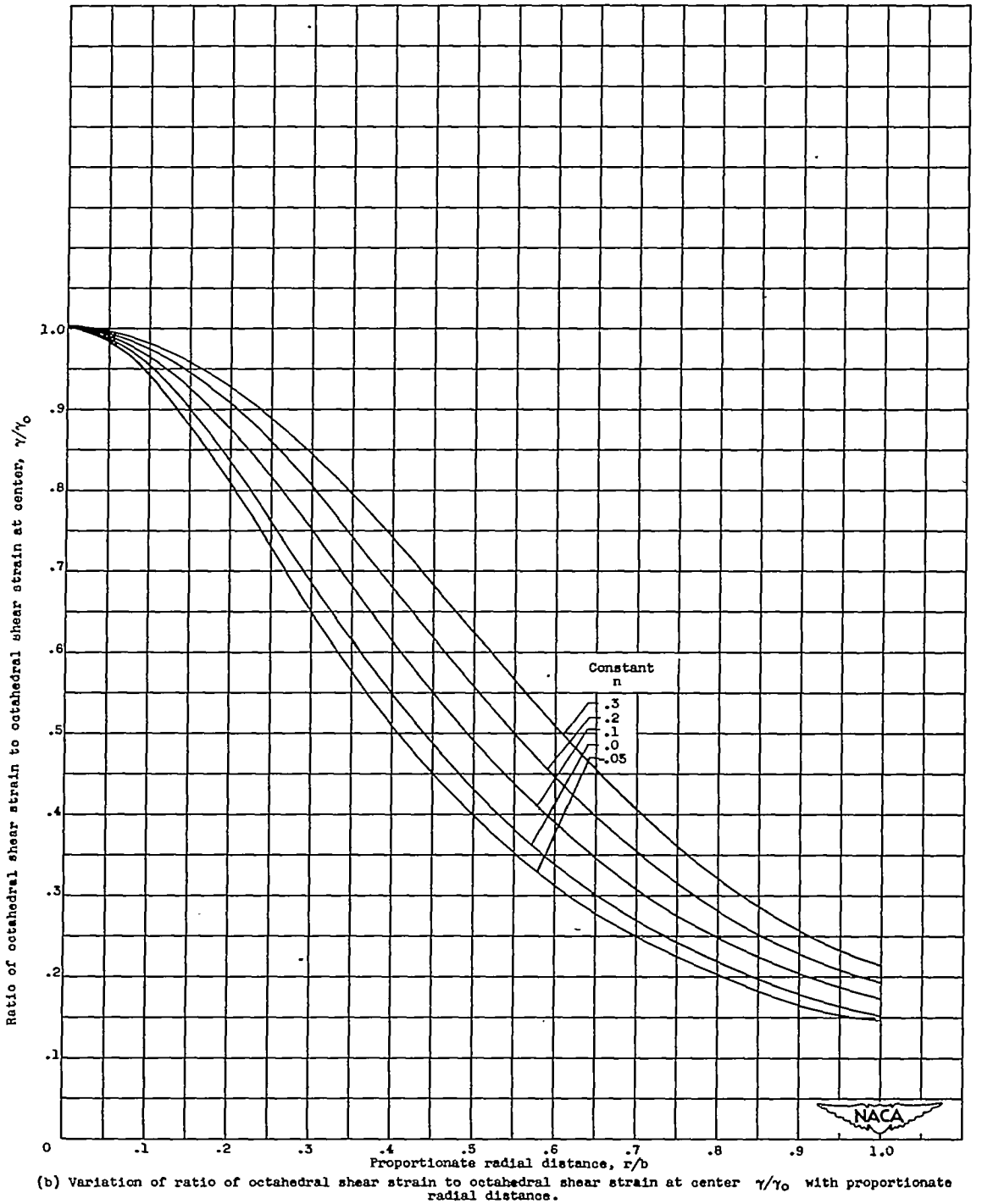

(b) Variation of ratio of octahedral shear strain to octahedral shear strain at center γ/γ_o with proportionate radial distance.

Figure 4. - Concluded. Variations of parameter α and ratio of octahedral shear strain to octahedral shear strain at center γ/γ_o with proportionate radial distance r/b obtained by partly linearized solution for different values of n.

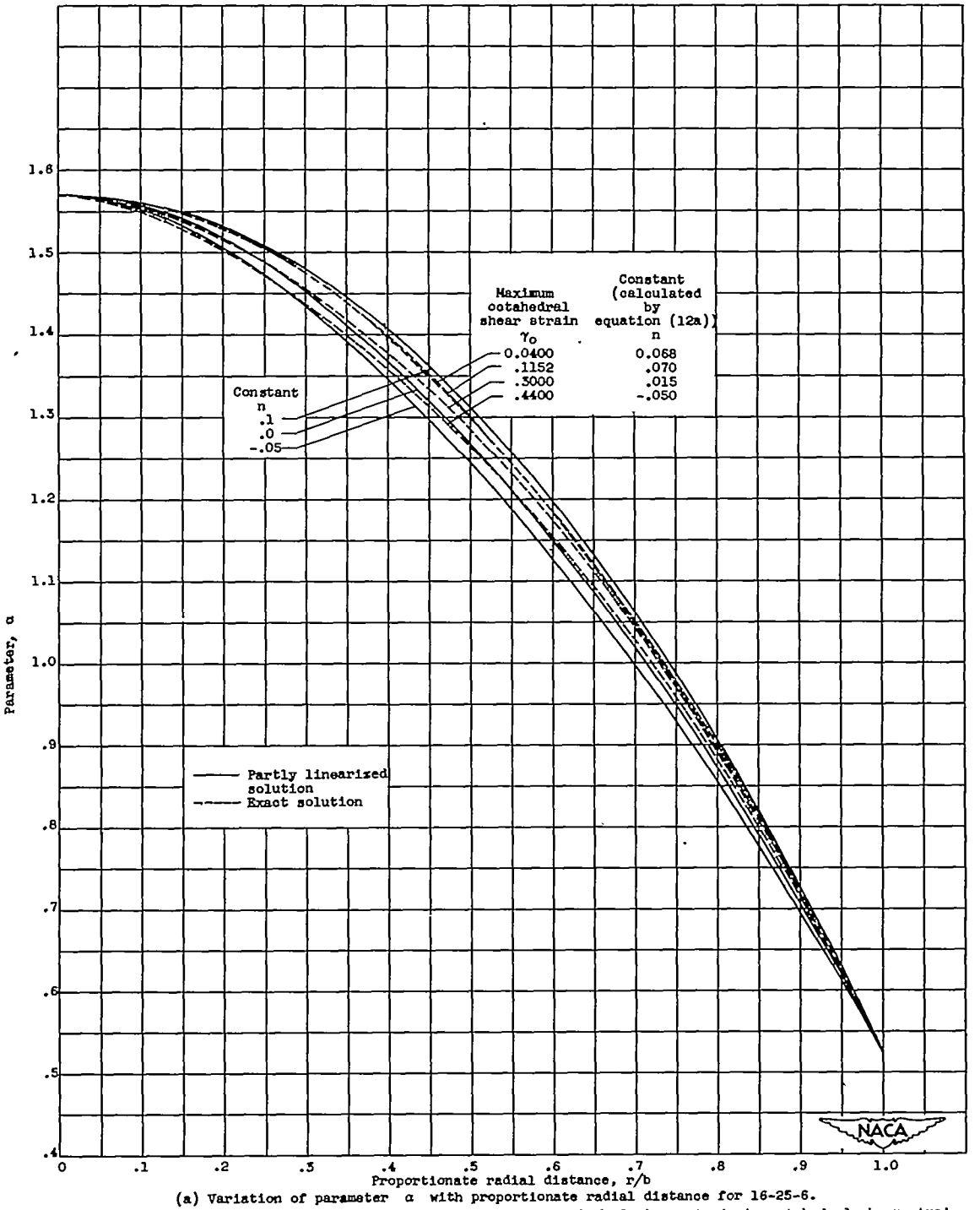

(a) Variation of parameter α with proportionate radial distance for 16-25-6.

Figure 5. - Comparison of variations of parameter α and ratio of octahedral shear strain to octahedral shear strain at center γ/γ_o with proportionate radial distance r/b obtained by partly linearized solution and by exact solution for 16-25-6 and Inconel X.

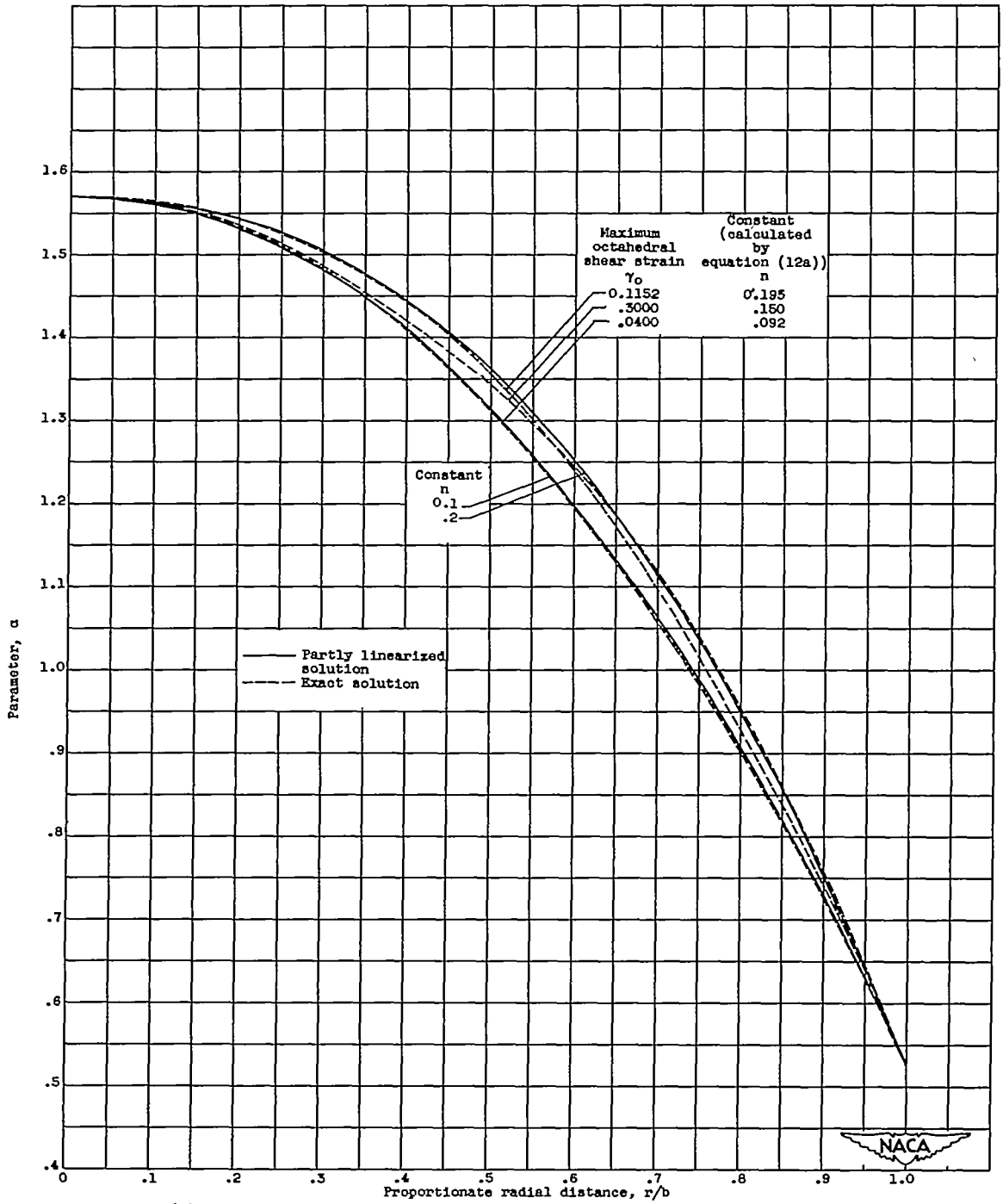

(b) Variation of parameter α with proportionate radial distance for Inconel X.

Figure 5. - Continued. Comparison of variations of parameter α and ratio of octahedral shear strain to octahedral shear strain at center γ/γ_o with proportionate radial distance r/b obtained by partly linearized solution and by exact solution for 16-25-6 and Inconel X.

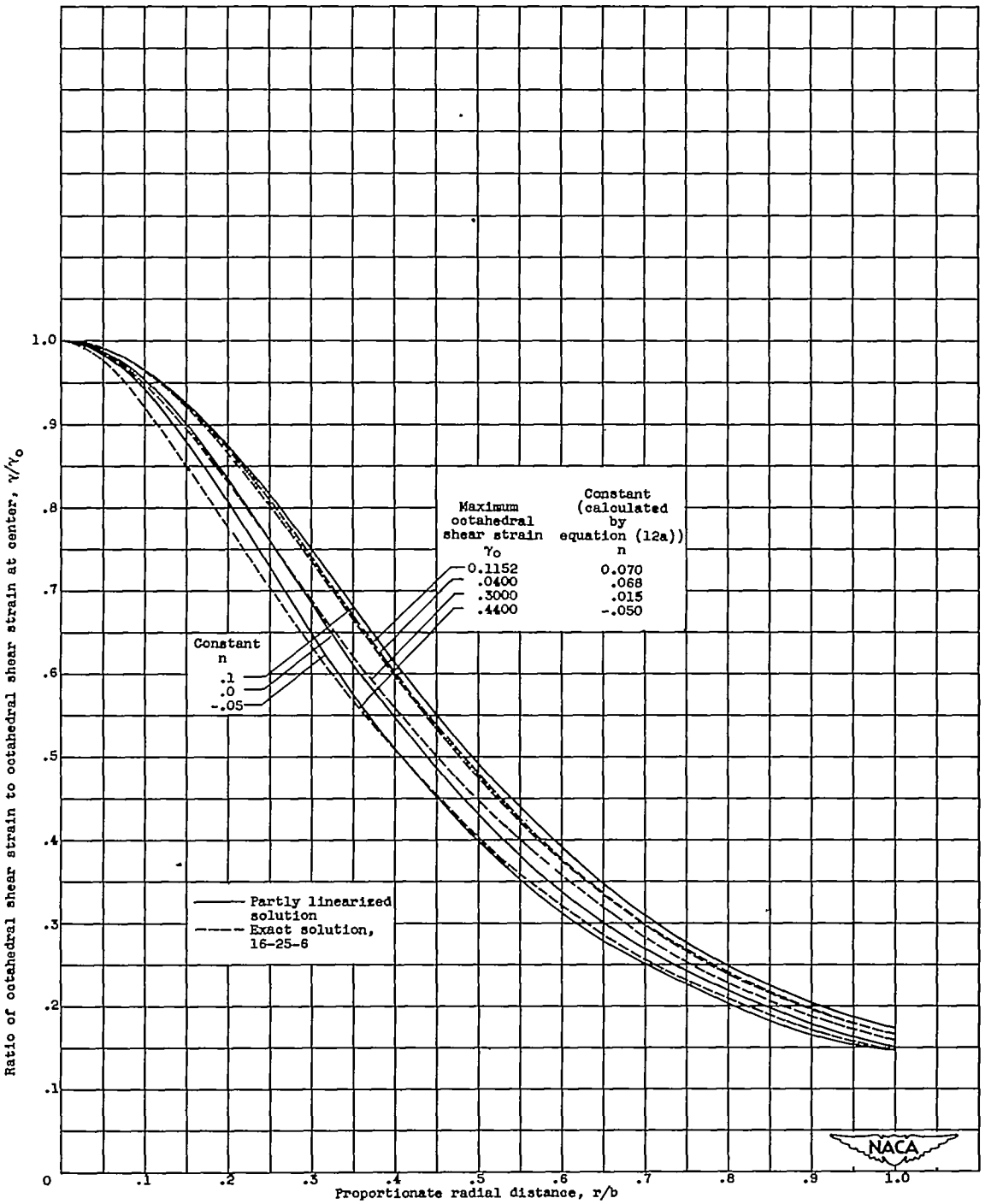

(c) Variation of ratio of octahedral shear strain to octahedral shear strain at center γ/γ_o with proportionate radial distance for 16-25-6.

Figure 5. - Continued. Comparison of variations of parameter α and ratio of octahedral shear strain to octahedral shear strain at center γ/γ_o with proportionate radial distance r/b obtained by partly linearized solution and by exact solution for 16-25-6 and Inconel X.

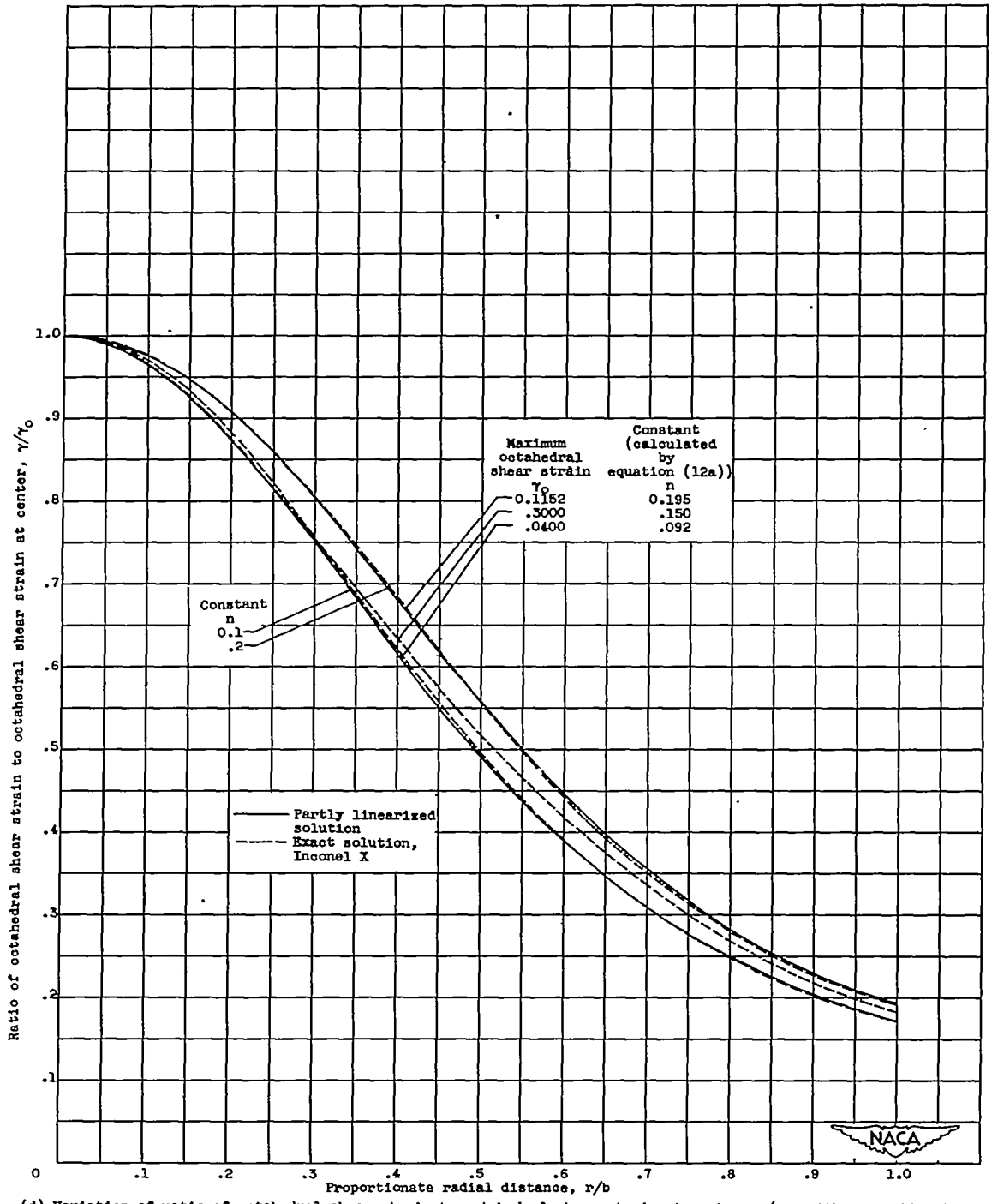

(d) Variation of ratio of octahedral shear strain to octahedral shear strain at center γ/γ_o with proportionate radial distance for Inconel X.

Figure 5. - Concluded. Comparison of variations of parameter α and ratio of octahedral shear strain to octahedral shear strain at center γ/γ_o with proportionate radial distance r/b obtained by partly linearized solution and by exact solution for 16-25-6 and Inconel X.

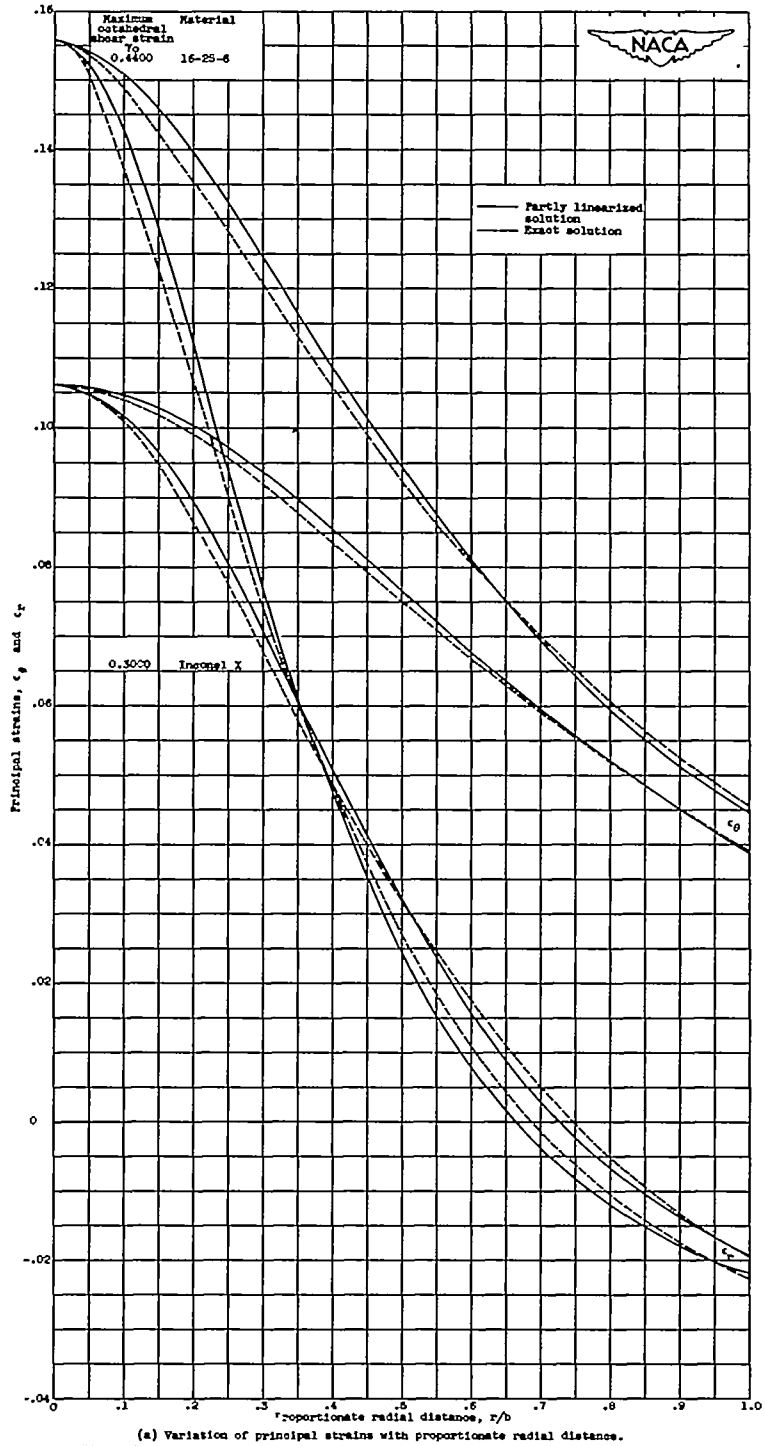

(a) Variation of principal strains with proportionate radial distance.

Figure 6. - Comparison of principal strains and stresses obtained by partly linearized solution and exact solution.

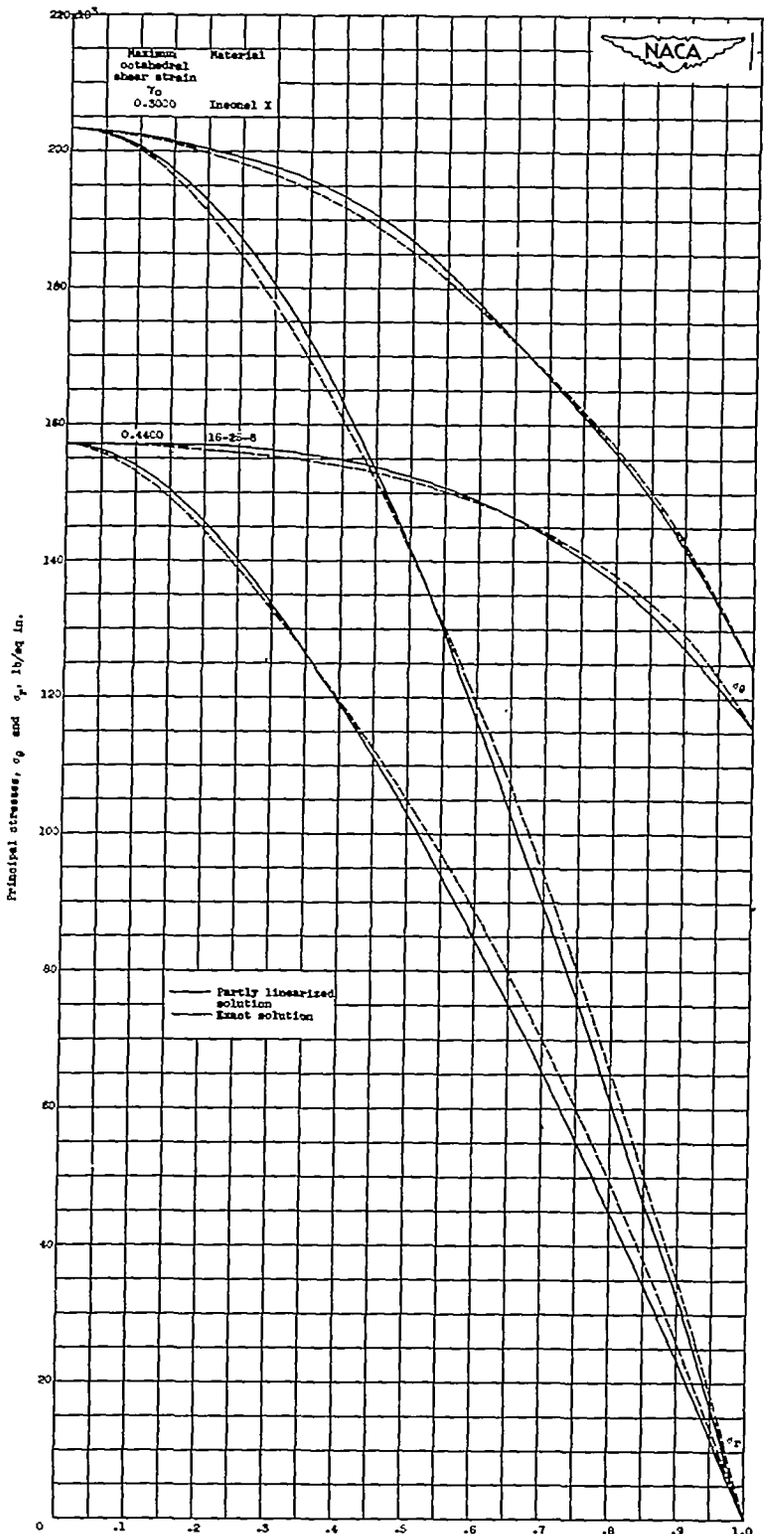

(b) Variation of principal stresses with proportionate radial distance.

Figure 6. - Concluded. Comparison of principal strains and stresses obtained by partly linearized solution and exact solution.

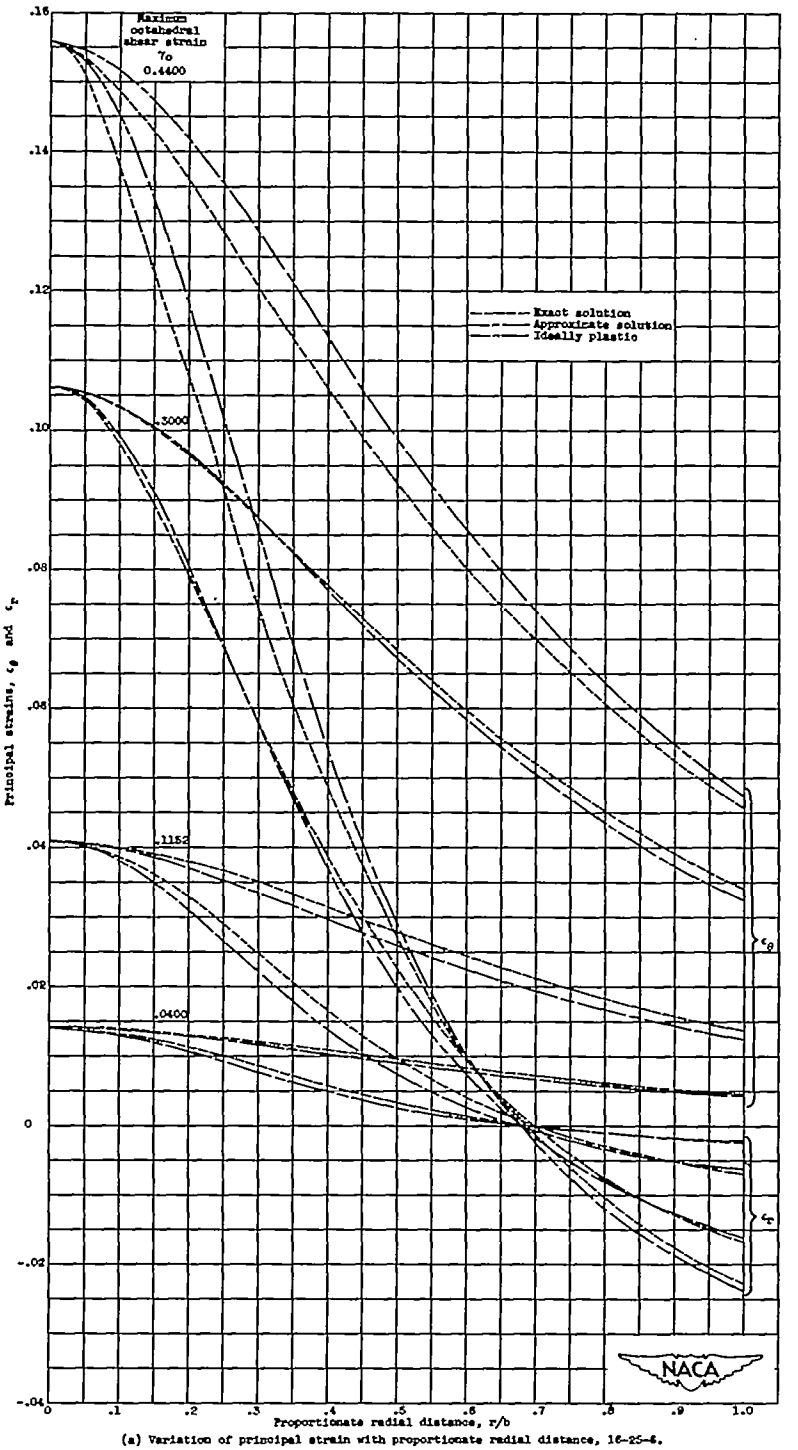

(a) Variation of principal strain with proportionate radial distance, 16-25-6.

Figure 7. - Comparison of principal strains and stresses obtained by approximate solution and exact solution.

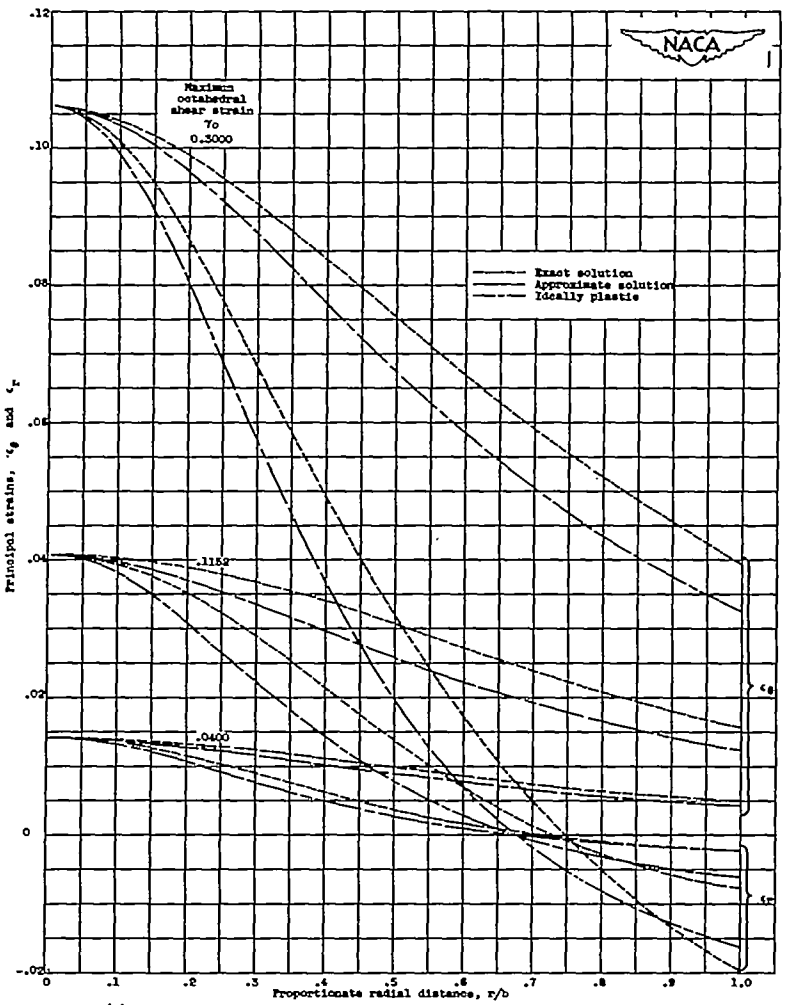

(b) Variation of principal strains with proportionate radial distance, Inconel X.

Figure 7. - Continued. Comparison of principal strains and stresses obtained by approximate solution and exact solution.

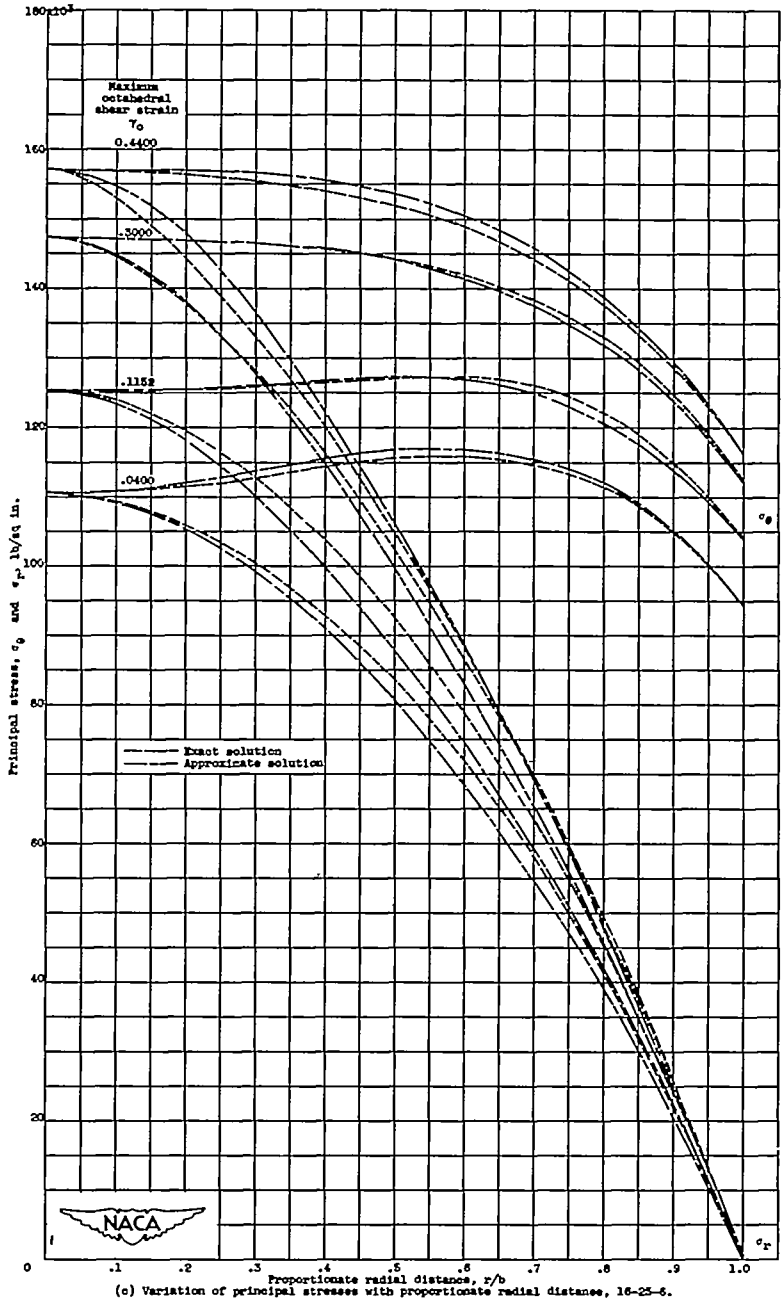

(c) Variation of principal stresses with proportionate radial distance, 16-25-6.

Figure 7. - Continued. Comparison of principal strains and stresses obtained by approximate solution and exact solution.

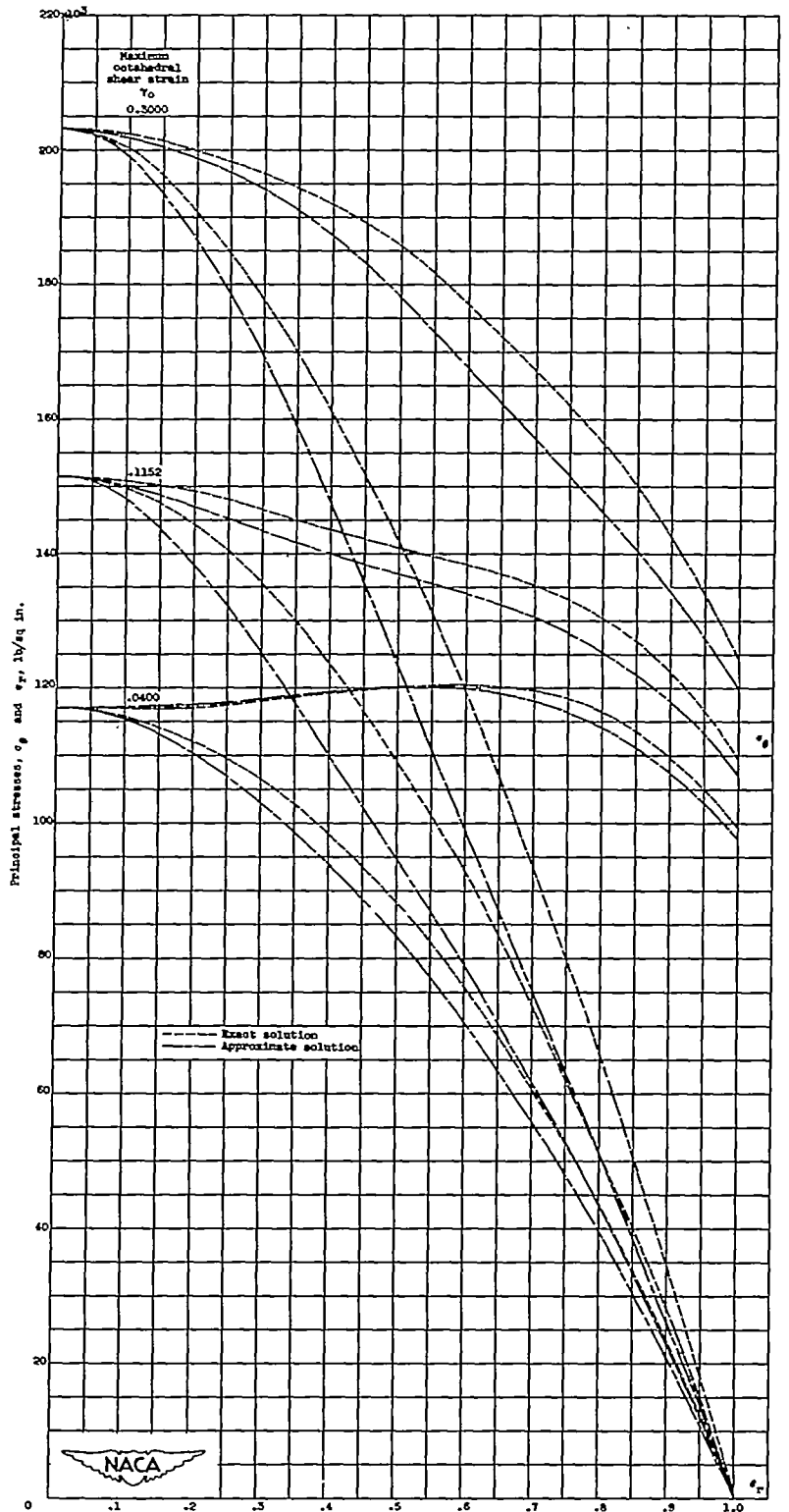

(d) Variation of principal stresses with proportionate radial distance, Inconel X.

Figure 7. - Concluded. Comparison of principal strains and stresses obtained by approximate solution and exact solution.

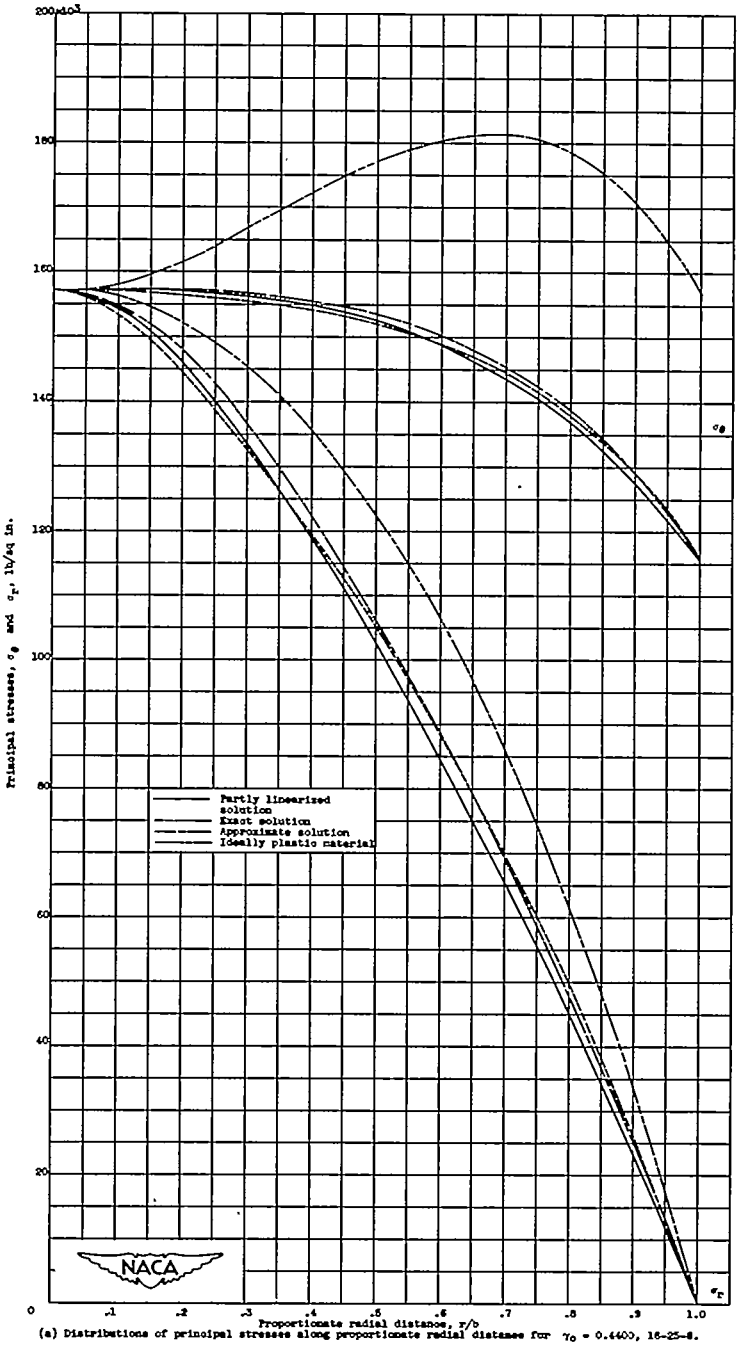

(a) Distributions of principal stresses along proportionate radial distance for $\gamma_0 = 0.4400$, 16-25-8.

Figure 8. - Comparison of principal stresses obtained by different methods.

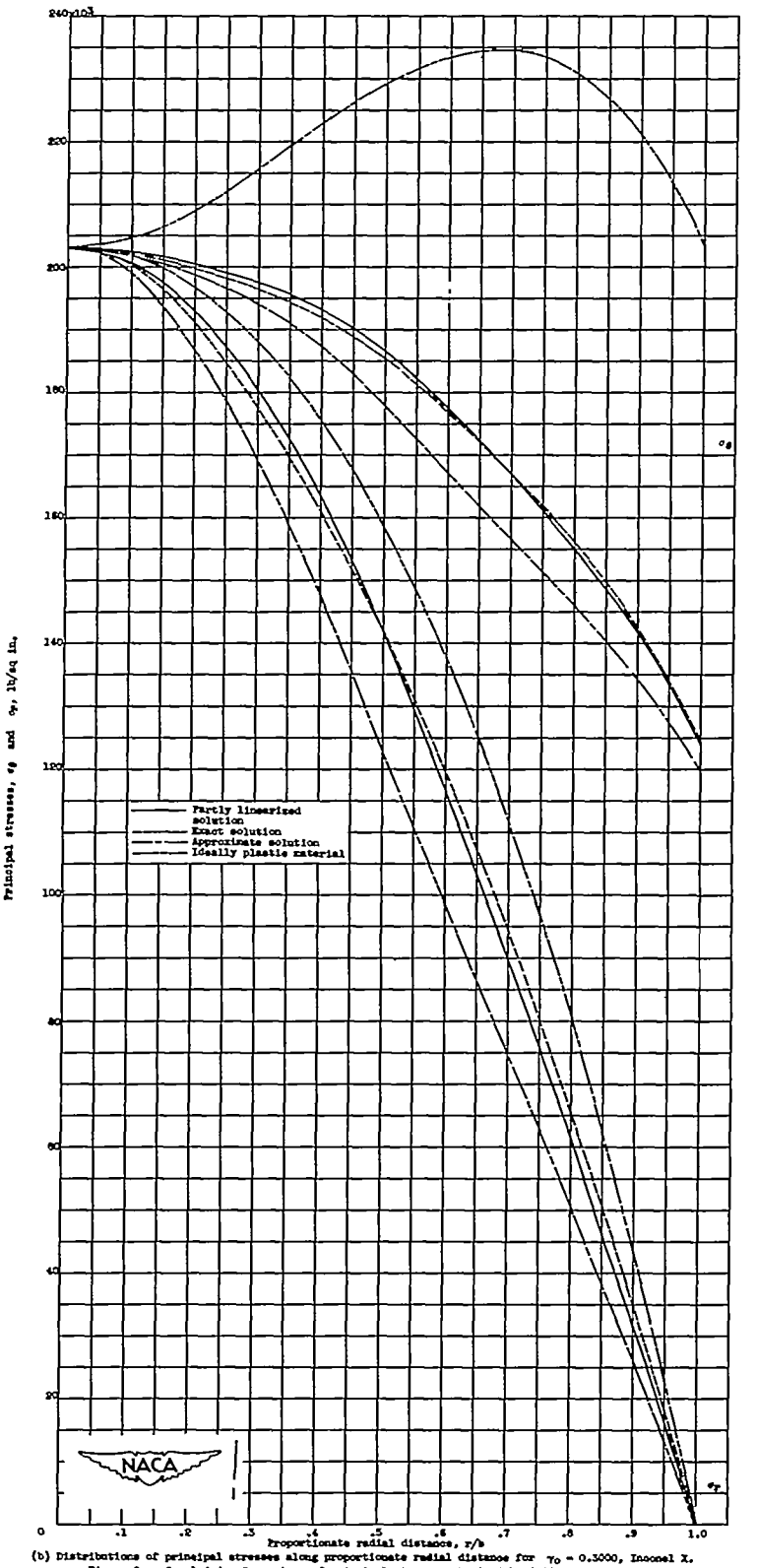

(b) Distributions of principal stresses along proportionate radial distance for $r_0 = 0.3000$, Inconel X.

Figure 8. - Concluded. Comparison of principal stresses obtained by different methods.

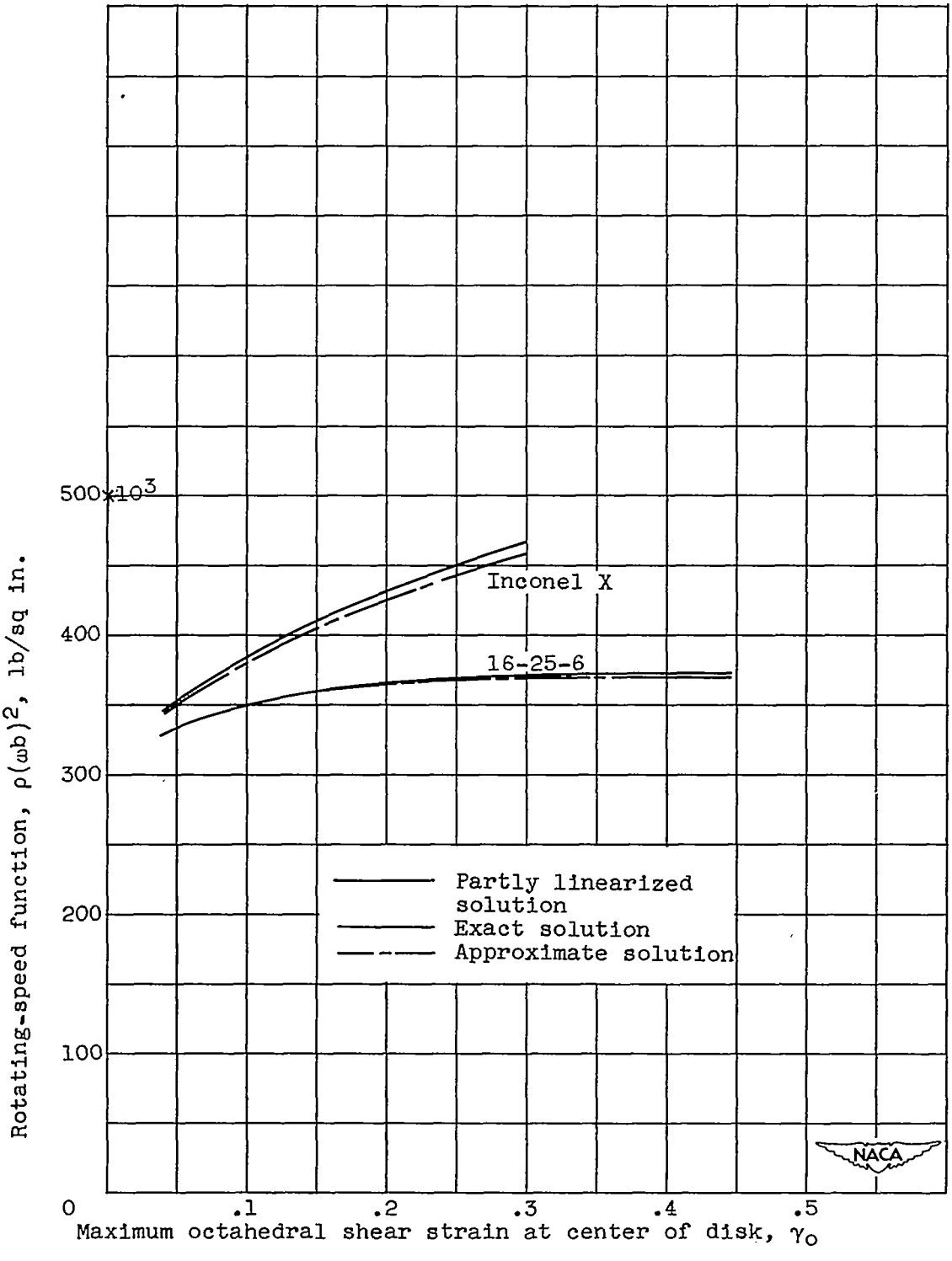

Figure 9. - Comparison of relations between rotating-speed function $\rho(\omega b)^2$ and maximum octahedral shear strain at center of disk obtained by exact, partly linearized, and approximate solutions for Inconel X and 16-25-6.

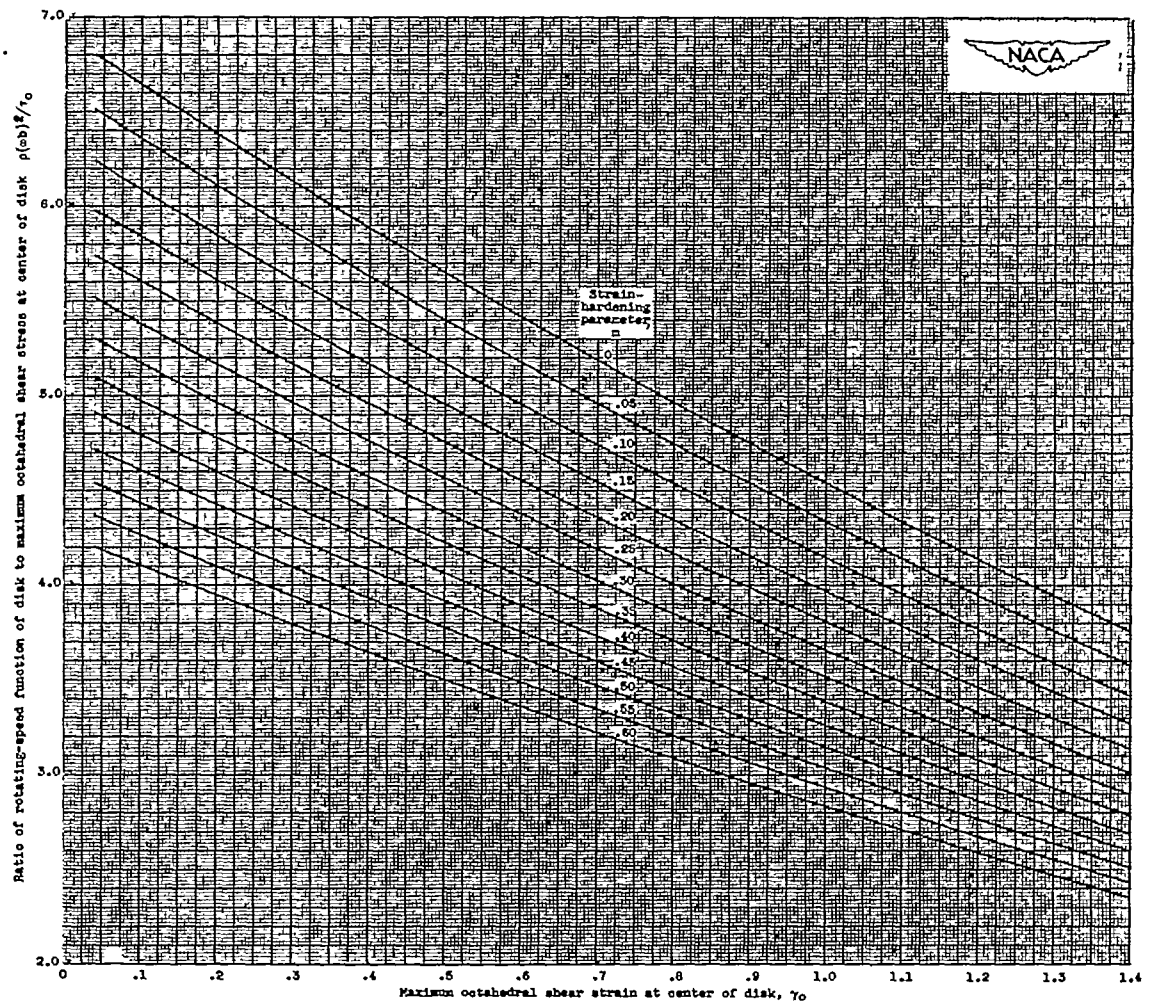

Figure 10. - Variation of ratio of rotating-speed function to maximum octahedral shear stress at center of disk $\rho(\omega b)^2/\tau_o$ with maximum octahedral shear strain at center of disk for different values of parameter m. (A 14- by 15-in. print of this fig. is attached.)

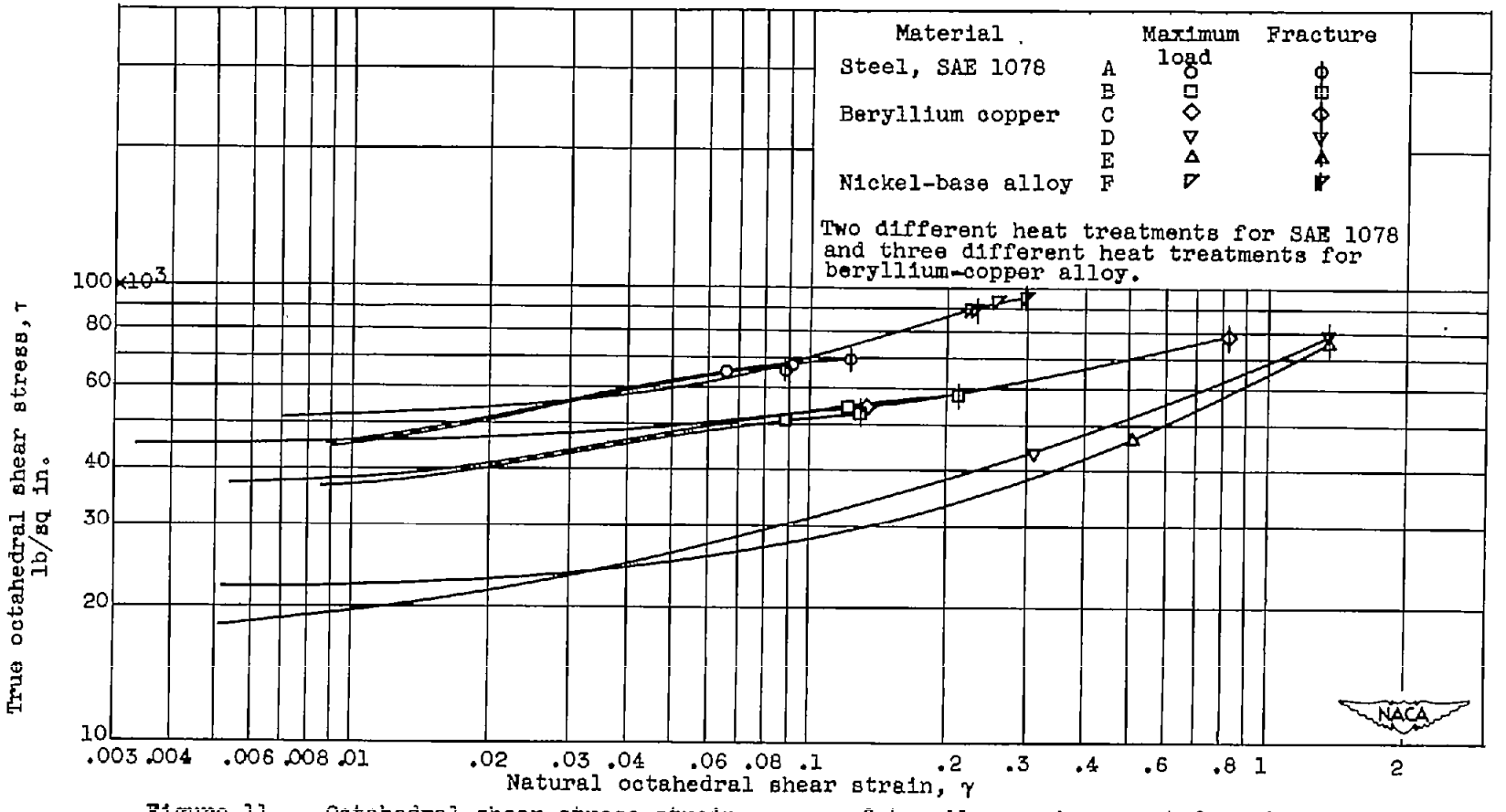

Figure 11. - Octahedral shear stress-strain curves of tensile specimens cut from disks.

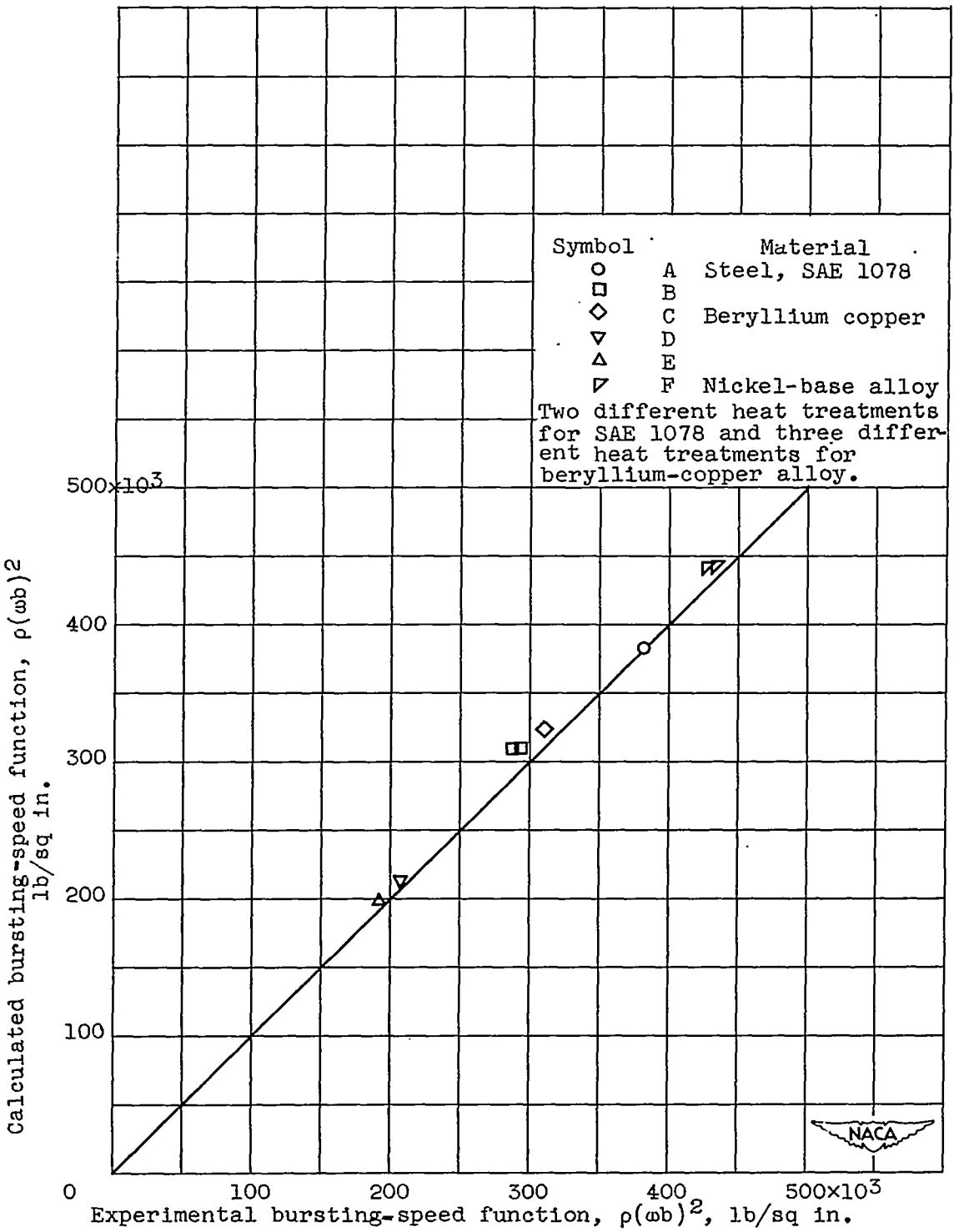

Figure 12. - Relation between calculated and experimental bursting speed function.